Chapter 5

Non-Vacuum Process for Production of Crystalline Silicon Solar Cells

Abdullah Uzum, Seigo Ito, Marwan Dhamrin and Koichi Kamisako

Additional information is available at the end of the chapter

http://dx.doi.org/10.5772/intechopen.68170

Abstract

Existing technologies for conventional high-efficient solar cells consist of vacuum-processed, high cost, sophisticated, and potentially hazardous techniques ($POCl_3$ diffusion, SiNx deposition, etc.) during crystalline silicon solar cell manufacturing. Alternative research studies of non-vacuum and cost-efficient processes for crystalline silicon solar cells are in continuous demand. However, there is not a well understanding of utilizing schemes and the achievable performances for such applications and techniques in solar cell fabrication. This chapter addresses the non-vacuum processes and applications for crystalline silicon solar cells. Such processes including spin coating and screen-printing phosphorus and boron diffusions for the formation of n+ and p+ emitter or back surface fields, spin coating and spray-deposited antireflection coatings for silicon solar cells. Application techniques were explained by combining and comparing experimental results with the calculation and simulations. Consequently, the aim of this chapter is to provide a good understanding of the non-vacuum processes for crystalline solar cells both with simulation and with experimental proves.

Keywords: low-cost solar cell, non-vacuum process, single diffusion selective, screen-printing, crystalline silicon

1. Introduction

Solar energy is one of the most interesting and practical alternative source of energy against the conventional fossil fuels. Crystalline silicon-based solar cells are dominant by far in photovoltaic industry and shares about 90% solar cell production worldwide. Low cost is still one of the main interests for the photovoltaic industry while stabilizing high conversion efficiency. Utilized materials and processing techniques are the major components that need to

be considered for cost reduction. A conventional p-type solar cell fabrication process basically comprises of texturing, n-type emitter formation (phosphorus diffusion), bulk passivation, antireflection coating, back surface field, and back/front metallization steps. Although, high-efficiency solar cells greater than 20% including record efficiencies [1] provide a good performance, they cannot demonstrate the feasibility for low-cost scale due to the complex structures and long and costly fabrication processes. Therefore, the efficiency of standard industrial cells still remains in the range of 15–20%. In order to meet industrial requirements with simple low-cost technologies with high throughput, cost-effective methods need to be investigated and adapted to the solar cell manufacturing process. By adaptation of such simple processing techniques including spin coating, spray deposition, and screen-printing methods with proper materials, high-efficiency solar cells that can be compatible with the commercial counter parts should be achievable. This study determines the ground for totally vacuum-free, low-cost crystalline silicon solar cell manufacturing process and applications.

2. Basic low-cost methods for film deposition

2.1. Spin-on deposition technique

The spin-on deposition (SOD) process generally applied by placing the substrate on the spinner and then the liquid source is dropped on the center of the wafer as shown in **Figure 1 (a)**. An optimized rotation speed is needed which depends on the size of the wafer and viscosity of solution, to avoid contamination on rear side of wafer. The coated wafer is usually baked on a hot plate in order to evaporate solvents (**Figure 1 (b)**) and to achieve a concrete layer. Then, the subsequent procedures such as thermal annealing at high temperatures, etc. might follow if necessary.

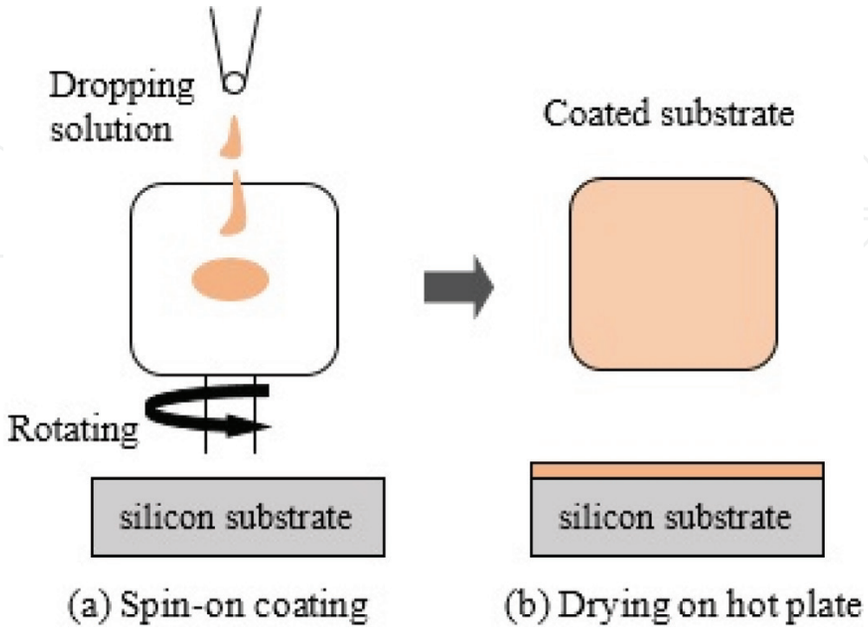

Figure 1. Spin coating technique. (a) Spin-on coating and (b) drying on hot plate.

Possibility of in-line processing for dopant sources to form semiconductor junctions, low energy consumption, simplicity, and low cost are the main advantages of SOD. For most of the SOD sources, low viscosity leads to homogeneous coatings even on textured samples but optimizations are usually necessary for a specific task. Depending on the SOD sources even storing in a refrigerator might be required, warming up to room temperature is usually necessary before the deposition process.

2.2. Screen-printing technique

Screen-printing is a fast, reliable, and cost effective technology which is used mainly for metallization purposes for silicon solar cell industry. The quality of the printing depends mainly on the parameters including the quality of printing mask, viscosity of the paste, snap-off distance, squeegee speed, scrapper pressure, squeegee pressure, and squeegee angle to the mask. For printing process, paste is forced through the openings of the emulsion layer onto the surface of the wafer. The printing mask consists of a frame that holds a stretched fabric with a photo stencil attached to the mesh with the required design of the grid pattern. That allows the transference of a diffusion ink or paste through a screen in a designed pattern on a silicon substrate located below and aligned with the pattern to be transferred as described in **Figure 2**.

The distance between the designed mask and the solar cell surface is called "snap-off" distance. It concerns with the vertical printing properties and by changing the snap-off distance, the pressure on the mask can be changed. The printing speed is also an important parameter and should be adjusted for each printing task because it affects the printed thickness/amount of the paste and the quality of the printing. Due to the increased applied force with increased printing speed, the print through process becomes easier. In order to achieve high throughput rates, a fast printing speed is required. Because the squeegee is the tool which contacts

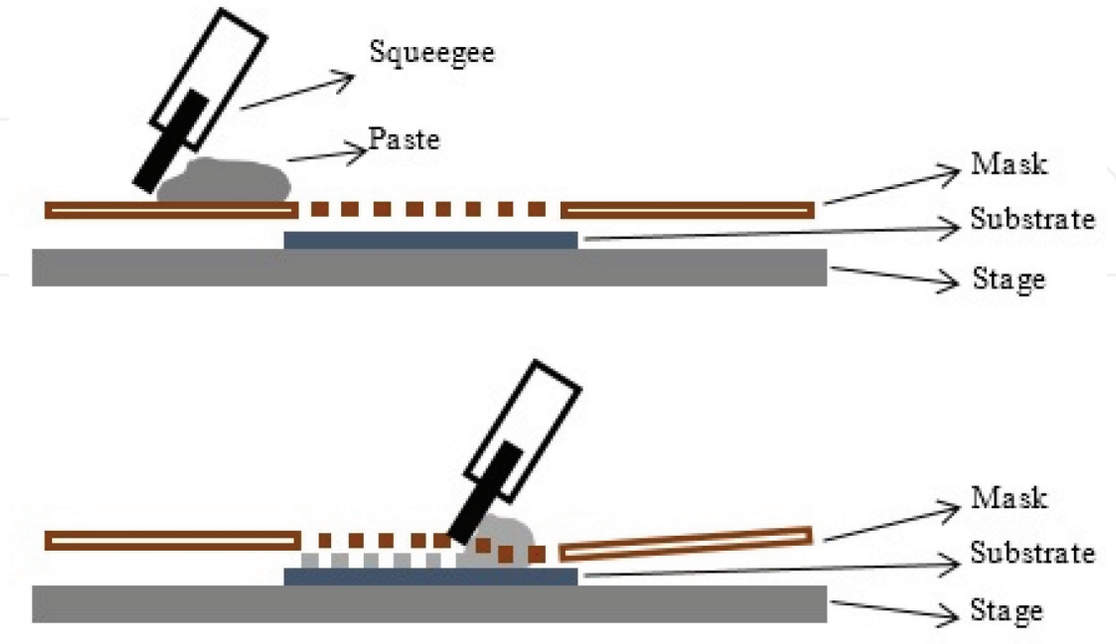

Figure 2. The moving of the squeegee and the deposition of the paste on the substrate.

directly to the mask and plays a key role on paste transfers through the mask. Hardness and the shape of the squeegee are needed to be considered. An excessive pressure on the squeegee results in a limited printing quality of fine-line printed contacts. It leads to an increased abrasion, and thus the lifetime of the screen-printing form and the squeegee is shortened. After the deposition of the paste on the surface, wafers are usually dried before the thermal annealing in case of the requirement of high temperature process. Besides the availability to form homogenous structures, the possibility of forming any designed structures in a simple way maybe the most attractive advantage for using screen-printing technique.

2.3. Spray deposition technique

Spray deposition technique is one of the low cost thin film-coating processes for solar cells. This technique is based on spraying particles of a precursor solution utilizing a spraying nozzle which can be controlled manually by a hand-pump or by automated pumping system. Fast processing, simplicity and low cost are the main advantages of spray deposition technique. In **Figure 3**, given an example setting schematic of spray deposition system, including spray nozzle, beaker for precursor solution, pipe which connects the pump to the nozzle and a manual or automated pump. The thickness of the coated films is usually controlled by the amount of precursor. And the uniform coating can be achieved by optimizing the height and facing angle of the nozzle to the substrate and the pressure of pumping. Generally, the homogeneity of the film can be altered by rotating the substrate in between each spraying pace. Considering the different materials and precursors, the substrate temperature is crucial. Therefore, pace of spraying in mL s^{-1} also needs to be taken into account.

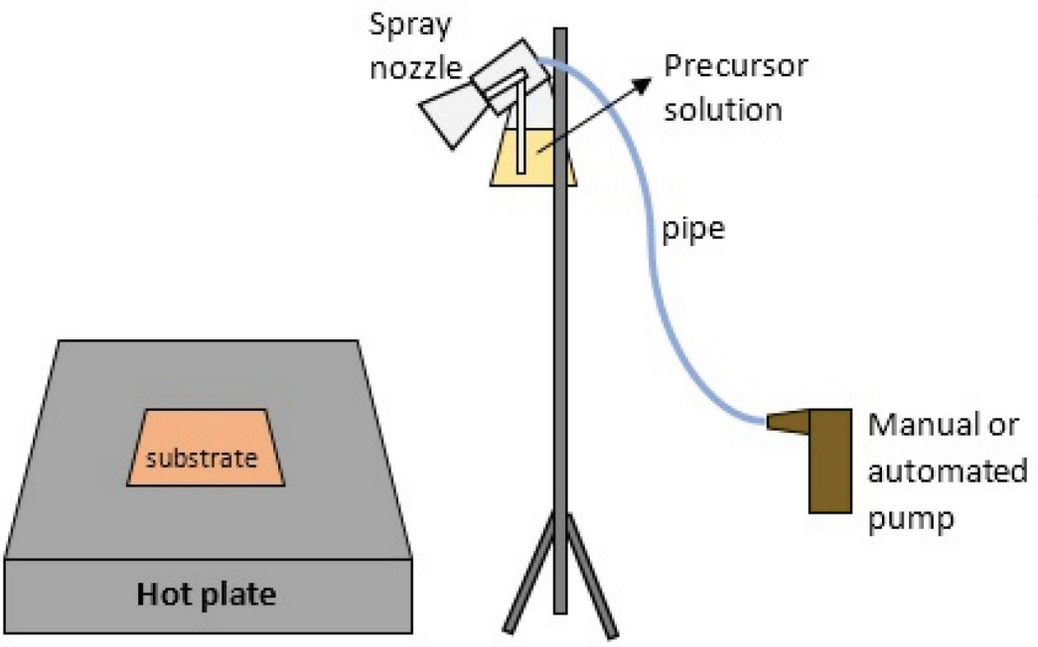

Figure 3. A schematic of a simple spray coating system.

3. Antireflection coating films for low-cost solar cells

In conventional crystalline silicon solar cells micrometer scale alkaline or acidic surface texturing is the primary method for light trapping into the solar cell. Additionally, antireflection coatings (ARC) are used to reduce the reflectivity. Various material and thin films have been used for ARC purposes including SiO_2, SiN_x, TiO_2, Al_2O_3 thin films, etc. SiN_x is the chief ARC film in conventional silicon solar cells industry with very good antireflective properties [2, 3]. SiN_x and its stack layers (e.g., SiN_x/SiO_x) are also used for passivation effect which leads higher carrier lifetimes [3]. These films are deposited by well-known plasma-enhanced chemical vapor deposition (PECVD) technique [4, 5] which has drawbacks including the need of toxic and hazardous gases such as SiH_4 and NH_3 with vacuum processing for CVD operation and considerably high costs. In order to meet industrial requirements with simple low-cost technologies with high throughput, cost-effective methods such as spin coating and spray deposition techniques are required to be investigated for crystalline silicon solar cell fabrication. Primarily, TiO_2 with good optical characteristics, found to be an attractive antireflection coating for solar cells [6, 7]. A considerable amount of literature has been published on sol-gel processes for silicon solar cells including TiO_2, TiO_2-SiO_2 [6, 7] and some Al_2O_3-based Ti doped mixed sol-gel sources as well have been introduced [8, 9]. On the other hand, ZrO_2 can be considered as a promising material for an antireflection coating of solar cells with high refractive index and thermal strength [10]. However, more research and analysis are needed to carry out for better understanding of this kind of material for adapting to the solar cell manufacturing.

3.1. Spin coating ZrO_2 film and TiO_2 films for ARC

3.1.1. Material optimization

In case of spin coating applications, development of spin coated material for a quality application while keeping desired electrical properties in a high-quality level is crucial for applications. Generally, nanoparticle processing makes it possible to utilize the solution processes for solar cells. Proper control of the material compositions and the applicability of low temperature processes are the main advantages. Investigating such kind of broad range of possibility of material and processes is important for solar cell manufacturing in terms of new material development, enhancement of the properties of a designed solar cell, especially the absorption of photons, and for cost reduction as well. This study consists investigation of colloidal suspension of ZrO_2 nanoparticles in water (ZR-30AH, provided by Nissan Chemical Industry Co. Ltd.), surface-modified colloidal suspension of TiO_2 nanoparticles in water (nanoUSE-Ti, Nissan Chemical Industry Co. Ltd.), and diluted TiO_2 nanoparticles (PST-18NR, provided by JGC Catalysts and Chemicals Ltd.). The average diameter of particles and the rate of solid components of ZrO_2 nanoparticles, surface-deactivated TiO_2-nanoparticles and TiO_2-nanoparticles are 50 nm (30 wt%), 13 nm (30 wt%), and 18 nm (17 wt%), respectively. Transmission electron microscopy (TEM) images of each nanoparticle were given in **Figure 4**.

Solutions for composite films were prepared by mixing one of the nanoparticles with ethanol and organic polymer of ethyl cellulose. For the preparation of ethyl cellulose, mixture of

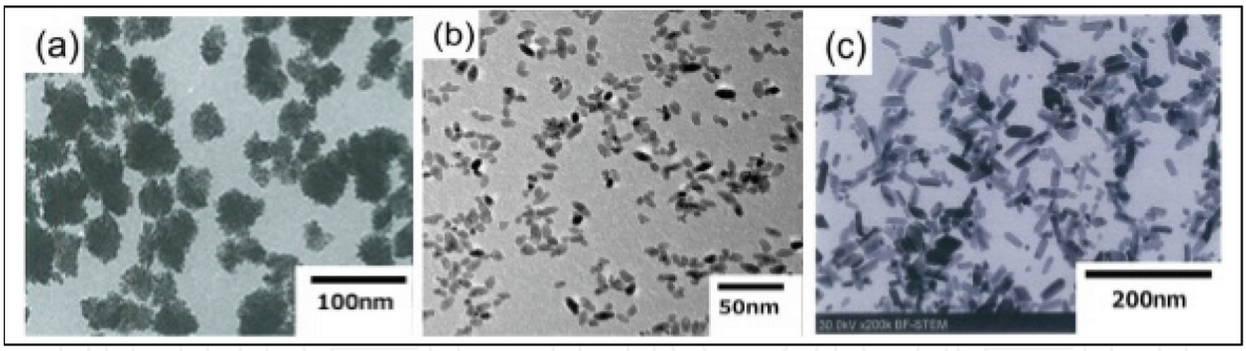

Figure 4. TEM images of nanoparticles of; (a) ZrO_2 (ZR-30AH, Nissan Chemical Industrial Co. Ltd.), (b) TiO_2 with surface deactivation (nanoUSE-TI, Nissan Chemical Industrial Co. Ltd.), and (c) TiO_2 (PST-18NR, JGC-CCIC Co. Ltd.) [11].

E0265 and E0266 (provided by Tokyo Chemical Industry Co. Ltd.) [11] was used. 50 g of E0265 and 50 g of E0266 were dissolved in 1 L of ethanol prior to mixing.

When solution process materials are aimed to be used for a specific purpose, the adaptation of the material for the process while achieving a quality physical and electrical properties are crucial. Considering the solar cell manufacturing process, textured surfaces are common for a solar cell to improve light trapping. Therefore, an ARC film needs to be applied smoothly to such surfaces for better spectral response. The nanoparticle-polymer composite layers formed on flat or alkaline textured crystalline silicon (c-Si) substrates and evaluation of the coating films were carried out as an antireflection coating (ARC) films. Based on this consideration, zirconium bare solution was formed by spinning on the surface of the textured wafer without any additives with spin speed of 4000 rpm for 20 s (acceleration time is 4 s). Between the textured pyramids detrimental cracks were observed after drying, as shown in **Figure 5 (a)**. These cracks need to be avoided to form a quality film. A mixed solution with ethanol was used [11] in a volume of 1:1; however, cracks could not be avoided totally. A total crack-free forming of the films was achieved by using of ethyl cellulose [11].

The ratio of the mixture was adjusted to 1:32:2 (in volume) of ethyl cellulose, ethanol, and zirconium sol, respectively. Ethyl cellulose is a well-known and widely used polymer with good material properties which is suitable to utilize for quality films [12]. It dissolves well in ethanol that is crucial in this study [12]. Spin coating conditions was similar with that of previous experiments which were without ethyl cellulose. As shown in **Figure 5 (d)**, quality film with smooth surface could be achieved with ethyl cellulose included solution. (This solution is used for the rest of the study of ZrO_2-P composite films). The crack-free surface may be due to the contribution of ethyl cellulose in terms of elasticity of the film. As well as the good light permeability of the ethyl cellulose is a great advantage when using for ARC materials where the transparency is so important.

As another alternative solution-processed ARC material, TiO_2 was also investigated and adapted to solar cell processing. Similar optimizations were carried out for TiO_2 solution as that of previously explained for ZrO_2 solution. TiO_2 solution was mixed with various amount of ethanol and surface condition of textured silicon was examined. 2, 4, 6, or 8 mL of ethanol mixed into 1 mL TiO_2 solution (spin speed of 5000 rpm for 25 s). It was confirmed that TiO_2

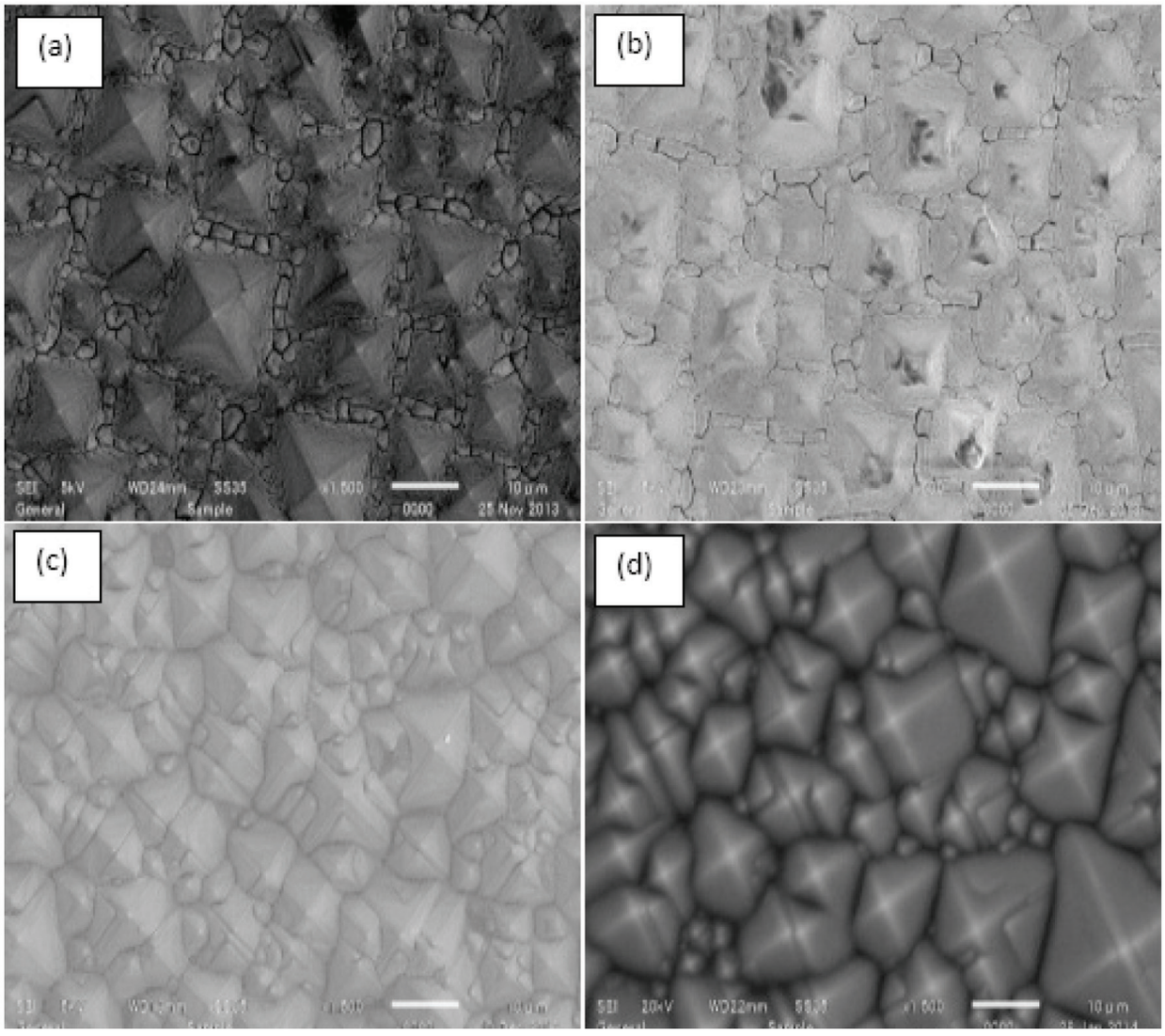

Figure 5. SEM surface images of antireflection coating on textured Si surface formed by ZrO_2 sol (with various amount of ethanol or ethylcellulose in 1 mL ZrO_2 sol); (a) pure ZrO_2 sol without ethanol or ethyl cellulose, (b) with 1 mL ethanol, (c) with 9 mL ethanol, and (d) with 8 mL ethanol + 0.25 mL, 10% ethyl cellulose solution in ethanol [11].

solution mixed with 8 mL of ethanol combination provided crack-free surface as shown in **Figure 6 (d)**.

3.1.2. Sample preparation and characterization of thin films

Square-shaped p-type Si wafers (25 × 25 mm^2) were cut out from 6-inch CZ-Si p-type wafers for optical-based experiments. First, wafers were dipped into 20% HF for 1 min and soaked in ionized water. Then, UV/O_3 cleaning was carried out to achieve a completely cleaned surface. Optimizations of spin coating process were carried out with various spin speed-time profiles. After optimizations, 5000 rpm for 25 s with acceleration of 5 s found to be optimum in most cases for this work. After the deposition of the films by spin coating, annealing was carried out 125°C for 5 min. Scanning electron microscope (SEM) measurements (JSM-6510, JEOL),

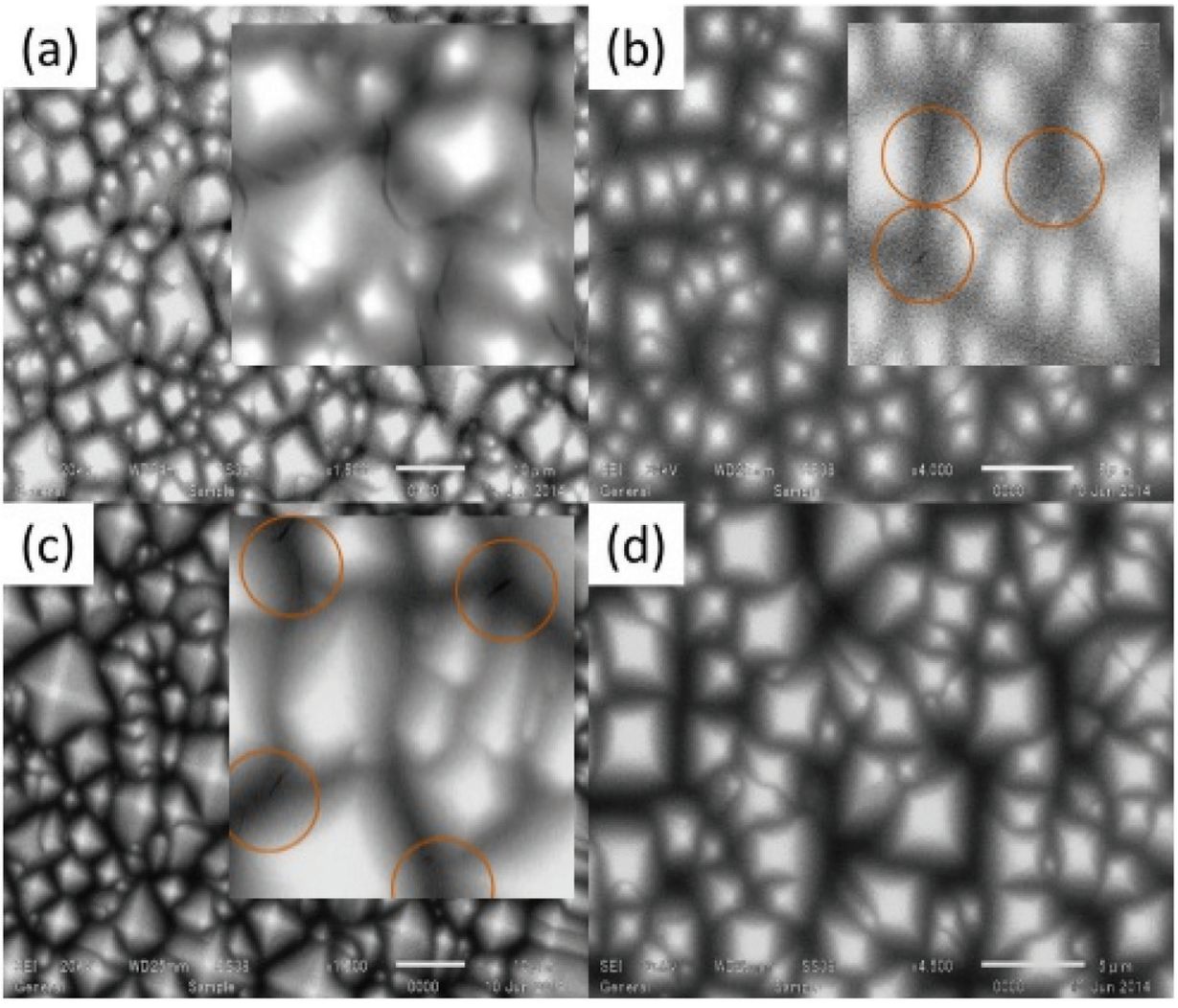

Figure 6. SEM surface images of antireflection coating on Si surface formed by surface-eliminated TiO_2 sol (various amount of ethanol in 1 mL TiO_2 sol); (a) with 2 mL ethanol, (b) with 4 mL ethanol, (c) with 6 mL ethanol, and (d) with 8 mL ethanol. The circles indicate the position of cracks [11].

reflection analysis (Lambda 750 UV/VIS Spectrometer, Perkin Elmer) and ellipsometer measurements (UviselErAgms-nds, Horiba Jobin Yvon) were mainly used for the analysis. C-Si solar cells were fabricated and analyzed as well.

Applied spin speed for thin film formation is important for a homogeneous formation of the thin film. The control of the film thickness is mainly established by the spin speed for spin coating applications. Reflection spectrometry is used for absorption, reflectivity, and transmission analysis which measures the absorbed portion of the photons as a function of wavelength. In case of an ARC material for silicon solar cells, it is important to analyze the characteristics of the ARC film by comparing the reflection on bare flat silicon surface, on bare textured silicon surface and such structured surfaces with applied ARC film. **Figure 7 (a)** compares the reflectivity of flat silicon substrates with and without ZrO_2-P layer coated on the surface with spin speed of 1000–4000 rpm for 20 s (acceleration time is 4 s). The lowest average reflectance (the

reflectance average between the wavelengths of 300–1100 nm) of 28% was achieved by ZrO_2 coating with a spin speed of 1000 rpm, a steady reflectance tendency from wavelength of around 700–1000 nm can also be confirmed. Considering the reflection of bare silicon surface as 40%, decrease of surface reflection down to 28% owing to the formed ZrO_2 film on the flat silicon surface, can be confirmed.

The reflectivity of textured silicon wafers covered by ZrO_2-P composite film including different amount of ethanol from 6 to 10 mL in the solution, was measured. Average reflectance of 6.5% was observed as the lowest value, when film formed with 0.5 mL zirconium solution (5.71%vl) + 0.25 mL ethyl cellulose (2.85%vl) + 8 mL (91.4%vl) combined solution. **Figure 7 (b)** shows the reflectance dependence of alkaline textured silicon substrates coated with ZrO_2-P composite film for spin speed in a range of 500–3000 rpm. Decrease of reflectance can be confirmed when increasing spin speed. Average reflectance reaches below 7% at spin speeds of 1500 rpm. Similar optimizations were performed for the films coated by SD-TiO_2 solution, both on flat or textured silicon substrates. Amount of ethanol was changed from 4 to 10 mL, in 1 mL SD-TiO_2 solution + 0.1 mL ethyl cellulose mixture. First, the mixed solution was formed on flat silicon surface by spin coating and annealing was carried out at 125°C for 5 min on a hot plate. In **Table 1**, the average reflectance of flat silicon surface coated with surface deactivated TiO_2-ethylcellulose film is summarized for each amount of ethanol in the solution.

Films formed with precursor solution contains 8 mL of ethanol provides the lowest average reflectances. Average reflectances of 19.92 and 20.04% were observed when the films were formed by for spin speed of 5000 and 8000 rpm, respectively. The reflectivity of textured silicon surface coated with SD-TiO_2-P film by varying the amount of ethanol from 4 to 10 mL, is

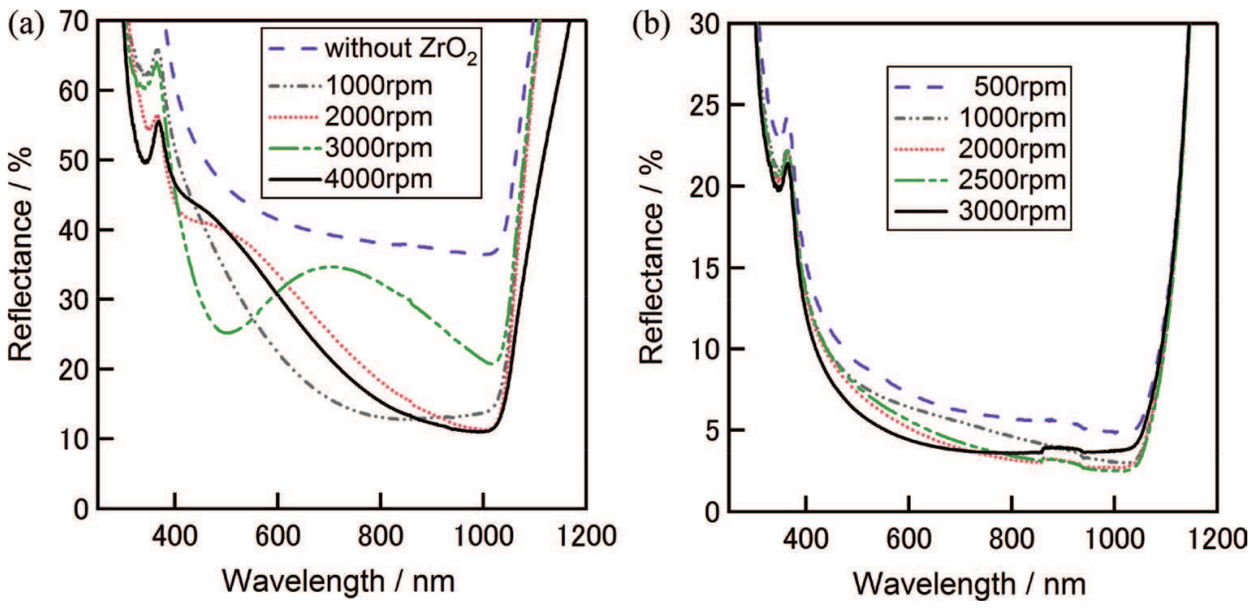

Figure 7. Reflectance spectra of flat surface silicon substrate with ZrO_2-polymer composite ARC; (a) by changing the spin-coat rotating speed and (b) reflectance of texture surface silicon substrate with ZrO_2-polymer composite ARC by changing the spin-coat rotating speed [11].

Speeds	EtOH (mL)			
	4	**6**	**8**	**10**
5000 rpm	30.00	24.00	19.92	22.66
8000 rpm	25.78	20.83	20.04	24.15

The volume of surface-deactivated TiO_2–sol was 1 mL [11].

Table 1. Average reflectance of flat silicon surface with surface-deactivated TiO_2-polymer ARC coating by different spin coating speeds.

given in **Figure 8**. Similarly as on flat silicon surface, the lowest average reflectance of 5.6% was achieved with the precursor contains 8 mL of ethanol.

3.1.3. Simulation and formation of ZrO_2-polymer/surface-passivated TiO_2-polymer composite multilayer film

Due to the difference on reflection of ambients and materials, photons come toward to surface of a solar cell experience three basic phenomenon: reflection, absorption, and transmission. In order to improve the efficiency of solar cells reflection must be minimized while absorption is maximized. It is known that multilayer structure of ARCs based on the gradual increase of each layer in the structure reflectance can be reduced significantly [13]. According to this fact, ⟨air/ZrO_2-polymer/surface-passivated TiO_2-polymer/Si⟩ multilayer structure was built with gradual of refractive indexes sequential order, as in $n_{air} < n_{ZrO2\text{-}polymer} < n_{TiO2\text{-}polymer} < n_{silicon}$.

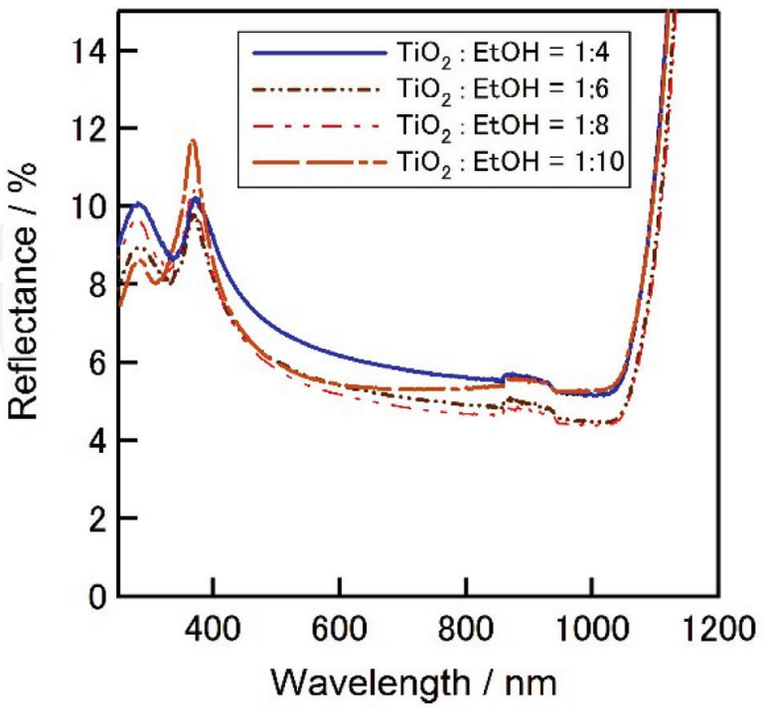

Figure 8. Reflectance spectra of textured silicon surface with surface-deactivated TiO_2-polymer antireflection coating [11].

Refractive indexes and extinction coefficients of ZrO_2-P and SD-TiO_2-P composite layers were achieved via fitting of ellipsometry measurements [11] as can be seen in **Figure 9 (a)** and **(b)**, where the refractive indexes of air and silicon are 1 and 4.3, respectively.

Only the absorbed photons can contribute on generation of electron-hole pairs where the reflected or transmitted photons are considered as energy loss. As the absorbed portion of total photons increases, the electrons moving to the conduction band increase thus contributes to the short-circuit current density (J_{sc}). Based on this basic fact, measured absorption-reflection spectra can be used to estimate J_{sc}. In order to determine this estimation Fresnel approach can be used. Fresnel equations describe the reflection and transmission behavior of photons regarding to a multilayer medium with different refractive indices [14]. Considering the refractive index, thickness of each layer and the transmission characteristics of a multilayer stack, it can be reduced down to a single imaginary layer by using Fresnel approach.

Follows a simulation study for the ⟨air/ZrO_2-polymer (ZrO_2-P)/surface-deactivated TiO_2-polymer (SD-TiO_2-P)/Si⟩ structure in order to estimate the short-circuit current density (J_{sc}). Thickness of the ZrO_2-P and SD-TiO_2-P composite layers were changed from 10 to 100 nm, and "incident photon to current conversion efficiency (IPCE)" was set to 100% for the calculation for the sake of achieving a comparable data. Eq. (1) was used to calculate J_{sc} to estimate optimum thicknesses of ZrO_2-P and SD-TiO_2-P composite films for a good multilayer ARC film.

$$J_{sc,max} \leq \frac{eS}{hc} \int_{300}^{1200} P_{in} \times Abs(\lambda)\ d\lambda \tag{1}$$

where $J_{sc,max}$ is maximum short-circuit current density (mA cm^{-2}), e is charge of an electron (1.602×10^{-19} A s), h is Plank's constant (6.626×10^{-34} eV s), c is speed of light (2.998×10^{8} m s^{-1}), P_{in} is the incident power in W m^{-2}, and λ is to denote wavelength (nm). Calculated J_{sc} values for ZrO_2-P/SD-TiO_2-P composite multilayer ARC films are given in **Figure 10**, and written down in detail in **Table 2**.

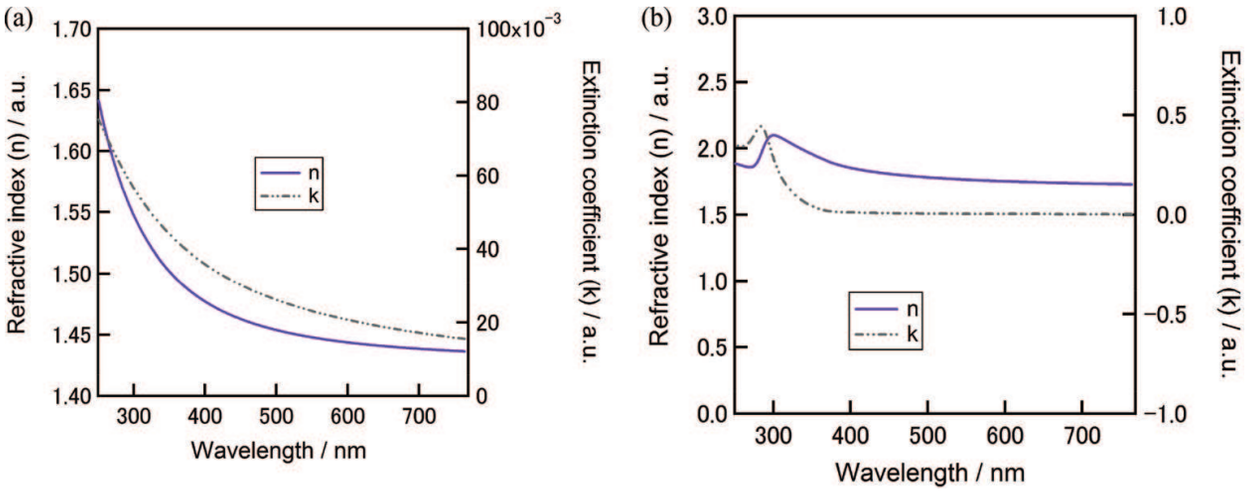

Figure 9. Fitting of ellipsometry measurements of (a) nano-colloid ZrO_2 (ZR30-AH)-polymer composite and (b) surface-deactivated TiO_2-polymer composite [11].

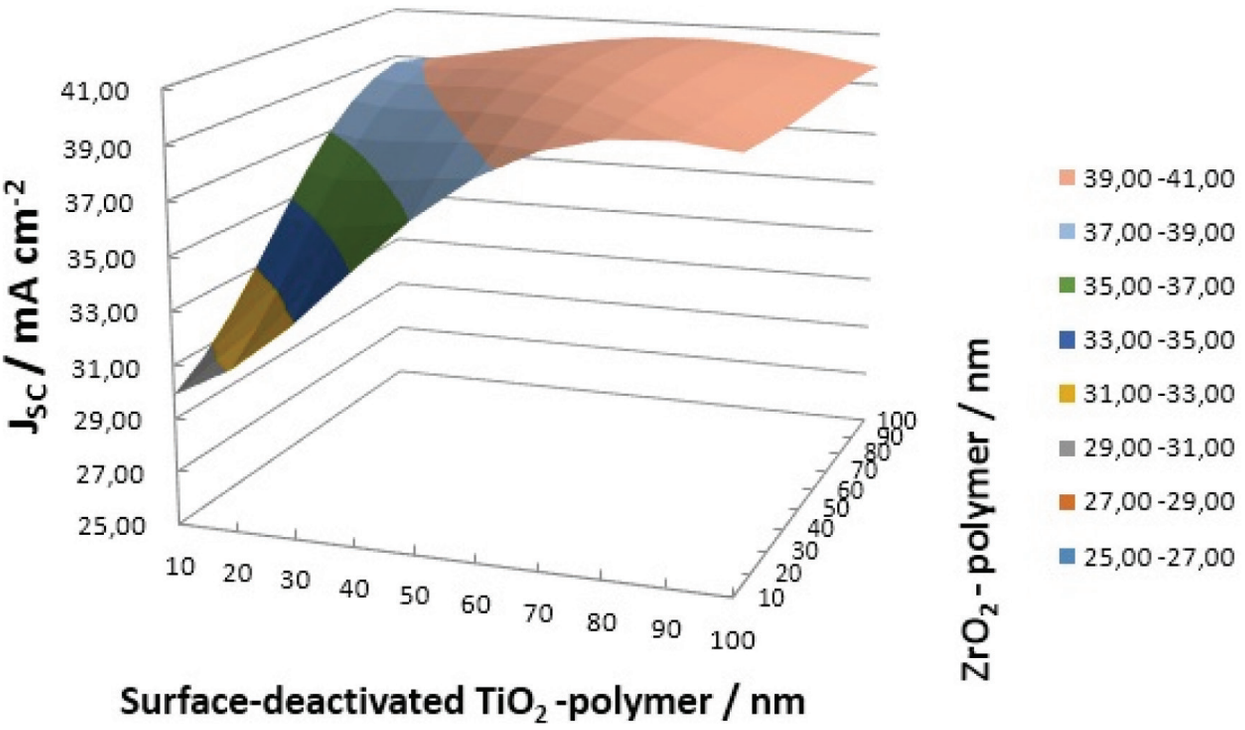

Figure 10. Estimated short-circuit current density with thickness variations of ZrO_2-polymer and surface-deactivated TiO_2-polymer films on flat-surface silicon solar cells [11].

ZrO_2/nm	TiO_2/nm									
	10	**20**	**30**	**40**	**50**	**60**	**70**	**80**	**90**	**100**
10	29.90	31.07	32.82	34.95	37.02	38.65	39.72	40.27	40.37	40.15
20	30.66	32.12	34.07	36.18	38.03	39.36	40.15	40.46	40.39	40.06
30	31.74	33.42	35.40	37.33	38.88	39.92	40.46	40.58	40.38	39.98
40	33.06	34.81	36.66	38.31	39.55	40.33	40.66	40.65	40.37	39.94
50	34.48	36.13	37.73	39.07	40.03	40.59	40.78	40.68	40.37	39.93
60	35.84	37.27	38.56	39.60	40.33	40.73	***40.83***	40.69	40.36	39.93
70	37.00	38.13	39.13	39.92	40.47	40.76	40.82	40.66	40.35	39.92
80	37.87	38.72	39.45	40.04	40.47	40.71	40.76	40.60	40.30	39.89
90	38.45	39.04	39.56	40.01	40.37	40.60	40.64	40.50	40.21	39.82
100	38.76	39.13	39.50	39.87	40.20	40.43	40.47	40.35	40.08	39.72

Table 2. Estimated short-circuit current density with thickness variations of ZrO_2-polymer and surface-deactivated TiO_2-polymer films on flat-surface silicon solar cells [11].

Highest J_{SC} of 40.83 mA cm^{-2} was confirmed with ⟨60 nm ZrO_2-P/70 nm SD-TiO_2-P⟩ composite multilayer ARC film. In experimental side of this investigation, such a multilayer film experimentally, first SD-TiO_2-P film was spin coated on the textured silicon surface and annealed at 125°C for 5 min, then the reflectance of the surface was measured. To form and characterize such a multilayer film experimentally, first SD-TiO_2-P film was spin coated on the textured silicon surface and then annealed at 125°C for 5 min, then the reflectance measurement was carried out. After the reflectance measurement of SD-TiO_2-P coated surface, ZrO_2-P film was spin coated on it and annealing was done similarly. **Figure 11** presents the comparison of reflectance spectra of ARC films on textured silicon surface of SD-TiO_2-P or ZrO_2-P/SD-TiO_2-P composite. Average reflectance of around 5.5% is achieved owing to the multilayer-structured ARC where the average reflectance of the surface without ARC was 16.3%.

3.1.4. Fabrication of p-type crystalline silicon solar cells

p-type CZ-Si solar cells with surface area of 25 × 25 mm^2, with/without ZrO_2-P or SD-TiO_2-P composite ARC layers and with/without ZrO_2-P/SD-TiO_2-P composite multilayer ARC, were fabricated. For textured solar cells, alkaline texturing was carried out [11] based on KOH solution in addition to Alka-Tex (provided by GP Solar) supporting agent at 80°C for 30 min. After the etching, all wafers were rinsed into 20% HF solution and soaked with ionized water.

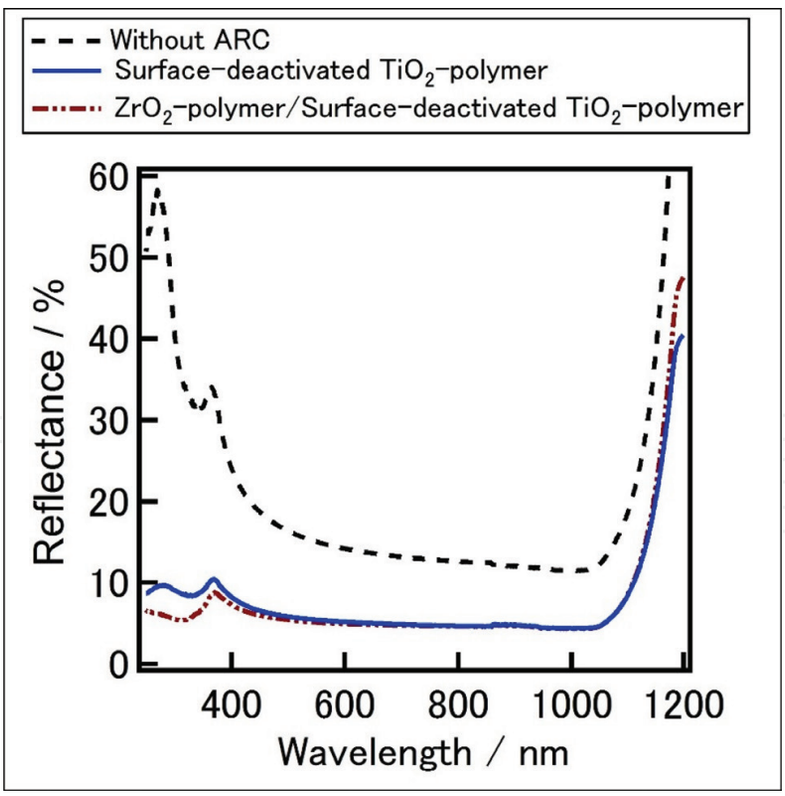

Figure 11. Reflectance spectra of textured silicon surface without ARC, with surface-deactivated TiO_2-polymer, ZrO_2-polymer/surface-deactivated TiO_2-polymer multilayer ARC [11].

For further cleaning, RCA cleaning process [15, 16] was carried out using a $NH_4OH/H_2O_2/H_2O$ (1:1:5 in volume) solution, at 80°C for 10 min. Follows a dip into 20% HF solution, and into $HCl/H_2O_2/H_2O$ (1:1:5 in volume) for 10 min at 80°C for a complete cleaning process. Prior to phosphorus diffusion, back side of the wafers were coated by polysilazane to avoid diffusion of phosphorus on back side. Coating of polysilazane was performed at 1500 rpm for 20 s (two times subsequent), and annealed at 600°C for 60 min in ambient O_2. $POCl_3$ diffusion was carried out at drive in temperature of 900°C for 30 min in ambient N_2. Post diffusion phosphorus silica glass was removed by 10% HF solution and wafers were cleaned in ionized water. Screen-printing Ag and Al was used for front and back contacts, respectively and cofired at 780°C for 1 min. ARC films were formed after the firing step by spin coating at 5000 rpm for 25 s) and annealing was carried out at 125°C for 5 min. For the cells with ZrO_2-P/SD-TiO_2-P composite multilayer structure ARC, first SD-TiO_2-P composite film was deposited and annealed and then ZrO_2-P composite film was deposited and annealed. The electrical characteristics of the fabricated solar cells with or without ZrO_2-P composite ARC are summarized in **Table 3**.

Best efficiency on flat surface silicon solar cell without ARC was 7.25% with J_{sc} of 24.03 mA cm^{-2}. After applying ZrO_2-P composite ARC, conversion efficiency increases up to 9.78% with J_{sc} of 30.22 mA cm^{-2} due to the formed ARC layer. In case of textured silicon solar cells, the conversion efficiency of solar cells without ZrO_2-P ARC increases from 10.2 up to 10.9%, where the J_{sc} were 28.74 and 30.62 mA cm^{-2}, respectively. This change is mainly due to the combined antireflection effect of textured surface and ZrO_2-P composite ARC layer.

On the other hand, considering the fabricated solar cells with SD-TiO_2-P ARC and ZrO_2-P/SD-TiO_2-P composite multilayer ARC, improvement of J_{sc} up to 32.44 and 33.00 mA cm^{-2} can be confirmed comparing to the J_{sc} of those of solar cells without ARC which was 30.93 mA cm^{-2}, respectively (values are average of three cells). Comparing the average efficiencies of the cells without ARC (11.99%) with those cells with ZrO_2-P/SD-TiO_2-P composite multilayer

ARC	Surface structure	*Jsc* (mA cm^{-2})	V_{oc} (V)	*FF* (%)	η (%)
Without ARC	Flat	24.03	0.527	57.1	7.25
With ZrO_2-polymer composite	Flat	30.22	0.537	60.2	9.78
Without ARC (textured ref 1)	Textured	28.74	0.511	69.4	10.20
With ZrO_2-polymer composite	Textured	30.62	0.510	69.7	10.89
Without ARC (textured ref 2)	**Best**	**29.33**	**0.570**	**71.7**	**11.99**
	Average	30.93	0.569	63.1	11.06
With surface-deactivated TiO_2 polymer	**Best**	**30.90**	**0.574**	**72.3**	**12.84**
	Average	32.44	0.575	63.7	11.84
With ZrO_2-polymer/surface-deactivated TiO_2 polymer	**Best**	**31.42**	**0.575**	**71.5**	**12.91**
	Average	33.00	0.574	62.7	11.85

Table 3. Photovoltaic characteristic of fabricated silicon solar cells on flat or textured silicon surface, with or without ZrO_2-polymer ARC.

ARC (12.85%), the improvement with an increase of J_{sc} (2.07 mA cm^{-2}) is worthfull. The best cell with ZrO_2-P/SD-TiO_2-P composite multilayer ARC is stand alone with the electrical characteristics of; J_{sc} of 31.42 mA cm^{-2}, V_{oc} of 575 mV, fill factor (*FF*) of 71.5%, and efficiency of 12.91%. **Figure 12** presents the *J-V* curve comparisons for best cells from each group of **Table 3**. From these results, the potential of spin coating ZrO_2-P, SD-TiO_2-P ARC and ZrO_2-P/SD-TiO_2-P based ARC on enhancing the optical performance of solar cells could be confirmed which can be a promising ARC candidate for the aim of low-cost silicon solar cells. For further analysis Ref. [11] can be referred.

It is worthy to note that better performances can be achieved especially on V_{oc} and on *FF*, with using high lifetime high quality wafers, a good bulk passivation and with a proper edge isolation.

3.2. Spray deposited TiO_2 and spin coating ZrO_2 films for ARC

In this part, spray deposited compact TiO_2 layer as a single layer ARC and spin-coated ZrO_2/spray deposited TiO_2 films as a double-layer ARC will be analyzed based on our previous work [17]. A compact TiO_2 film is commonly used for dye synthesized solar cells and perovskite solar cells between the front contact and porous TiO_2 layer to block the electron recombination which boost the current [18, 19]. This phenomena and adaptation of compact TiO_2 film to the silicon solar cells as an ARC will be discussed.

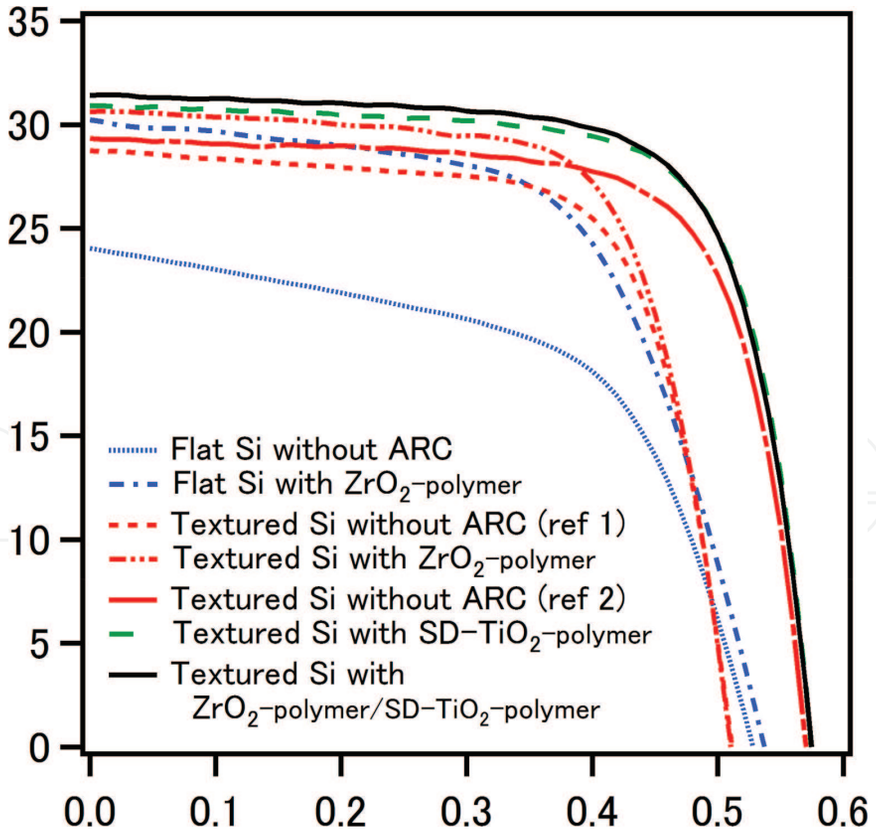

Figure 12. *J-V* curve of the best fabricated solar cells without any ARC film and with ZrO_2-polymer composite, with surface-deactivated TiO_2-polymer composite or ZrO_2-polymer composite/Surface-deactivated TiO_2 polymer-composite multilayer structure ARC films.

3.2.1. Sample preparation

p-type silicon wafers (25 × 25 mm^2) were cut out from 6-inch CZ-Si p-type wafers for the optical measurements. First, all wafers were dipped into the 20% diluted HF for 1 min and rinsed in distilled water. Afterwards, UV/O_3 surface treatment was carried out for a complete cleaning process. ZrO_2-polymer composite film was deposited on silicon substrate by spin coating using the zirconium sol (ZR-30AH, provided by Nissan Chemical Industry Co. Ltd., Chiba, Japan). Optimized ZrO_2 solution as explained in title of 3.1.1 composed by ethyl cellulose, ethanol, and ZR-30AH in ratio of 2:16:1 (in volume) was used in this work as well. Deposition of the ZrO_2 film was carried out by spin coating with a spin speed of 1500 rpm for 25 s (acceleration time is 5 s). In case of TiO_2 compact film deposition, spray pyrolysis was utilized and homogenous films were established by spraying precursor solution using a glass atomizer. Prior to spraying process crystalline silicon wafers were set on a conventional hot plate and heated up until the surface temperature of the substrate reaches 450°C. The TiO_2 precursor solution was composed of titanium bis-isopropoxide bis-acetylacetonate (TAA) and ethanol (1:10%vl). Annealing temperature was optimized for TiO_2 as 450 and as 125°C for ZrO_2, respectively. Analyses were mainly carried out by reflection analysis (by ultraviolet-visible spectroscopy, Lambda 750 UV/VIS Spectrometer, Perkin Elmer, Waltham, MA, USA) and ellipsometer (UviselErAgms-nds, Horiba Jobin Yvon, Kyoto, Japan) and finally by the performance of the fabricated silicon solar cells with or without ARC.

3.2.2. Characterization of the films

In order to evaluate the reflectivity performance of single layer TiO_2-compact film, at first flat surface silicon wafers were used. The thickness of the TiO_2 film was mainly controlled by the spraying amount of TiO_2 precursor solution in a range of 0–12 mL as previously mentioned. **Figure 13 (a)** shows the comparison of the reflectivity of flat samples with or without TiO_2-compact film on silicon surface. Depending the film thickness, minimum of the reflectance (<2%) shifts toward to the longer wavelengths. A steep decrease before the minimum can be confirmed for all TiO_2 film coated surfaces. The minimum of the reflectance shifts to the wavelengths as high as around 1000 nm for the films coated with 10 and 12 mL TiO_2 precursors due to the thickening of the film. The average reflectivity (the reflectance average between the wavelength of 300–1100 nm) was plotted by changing the spraying amount of the TiO_2 precursor as 0, 2, 4, 6, 8, 10, and 12 mL, respectively (**Figure 13 (b)**). A deposition rate of TiO_2 is defined as 10.1 nm mL^{-1} according to ellipsometry measurements. The lowest average reflectance of 21.41% was achieved by spray-deposited TiO_2 coating with a thickness of 60.6 nm. These values are in a relative agreement of calculated value of 56.8 at the wavelength of 550 nm for the refractive index of TiO_2 as 2.2 [20]. The bottom of reflectance valley shifted to higher wavelength with increasing the solution volume from 2 to 12 mL, gradually which shows the thickness dependence of reflection as well. Using the 8 mL precursor solution, the second valley arouse at the lower wavelength which was close to the valley bottom of 2 mL precursor solution. The second valley at the lower wavelength was also shifted to the larger wavelength with increasing the amount of precursor solution.

http://dx.doi.org/10.5772/intechopen.68170

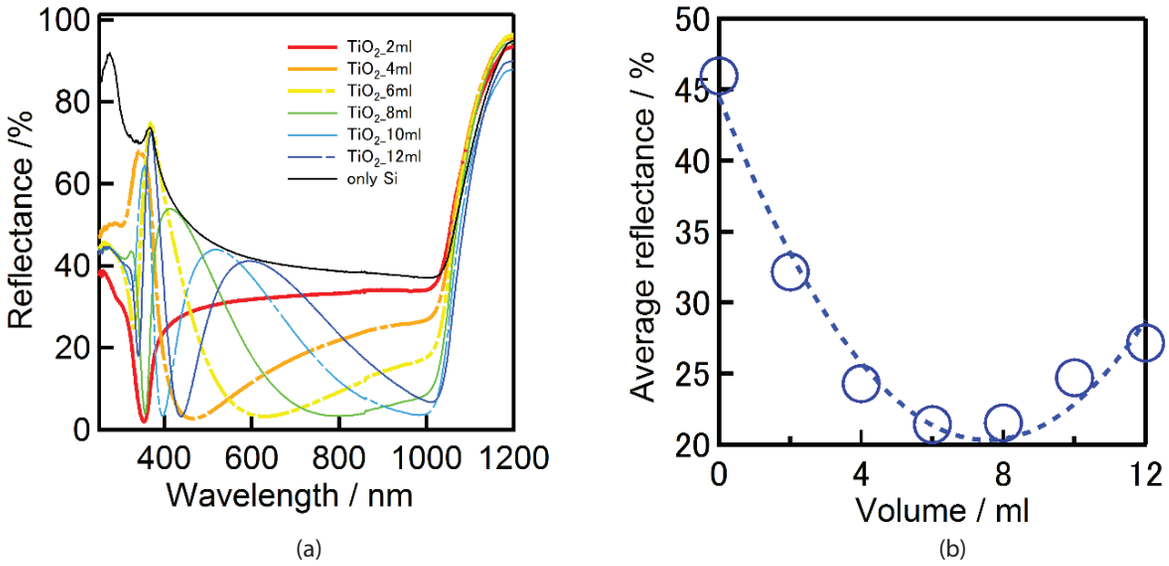

Figure 13. Comparison of the reflectivity of the flat samples with TiO_2 antireflection coatings by various amount TiO_2 precursor solution; (a) reflectance spectra depending to spraying amount and (b) average reflectance (300–1100 nm wavelength) depending to spraying amount [17].

In case of reflectivity measurement for ZrO_2-polymer composite/TiO_2-compact multilayer, first, TiO_2-compact single layer was formed and measured, then ZrO_2-polymer composite was formed on TiO_2 covered surface and remeasured. The comparison of reflectivity of TiO_2-compact single layer with the ZrO_2-polymer composite/TiO_2-compact multilayer formed on textured silicon wafers is given in **Figure 14**. The average reflectance was improved further with applying ZrO_2-polymer composite on the TiO_2-compact film, offering between 5 and 12% reflectance gain from 300 to 450 nm and a steady lower reflectance tendency from wavelength of around 700–1000 nm can also be confirmed.

3.2.3. Evaluation of the fabricated p-type crystalline silicon solar cells

Silicon solar cells were fabricated with a variety of final surface condition; without ARC on textured surface, with TiO_2-compact film on textured surface and with ZrO_2-polymer composite/TiO_2-compact multilayer ARC film on textured surface. For the fabrication of silicon solar cells, 25 mm × 25 mm p-type CZ-Si wafers were used as well. In this work, alkaline texturing process, RCA cleaning, UV/O_3 cleaning process, diffusion barrier of polysilazane forming were carried out in a similar way as explained in Section 3.1.4. $POCl_3$ diffusion was carried out at 930°C for 35 min in ambient N_2. Post diffusion PSG glass was removed by diluted HF and wafers were cleaned by ionized water. SiO_2 film was formed by thermal oxidation process at temperature of 800°C for 10 min under O_2 gas. Before the metallization process, wafers were set on a hot plate heated at deposition temperature (450°C) and deposition of TiO_2 films were carried out by spray pyrolysis. Then, front and back contacts were formed by screen-printing Ag and Al, respectively. Cofiring was carried out at 780°C for 1 min in an oven. After evaluating the solar

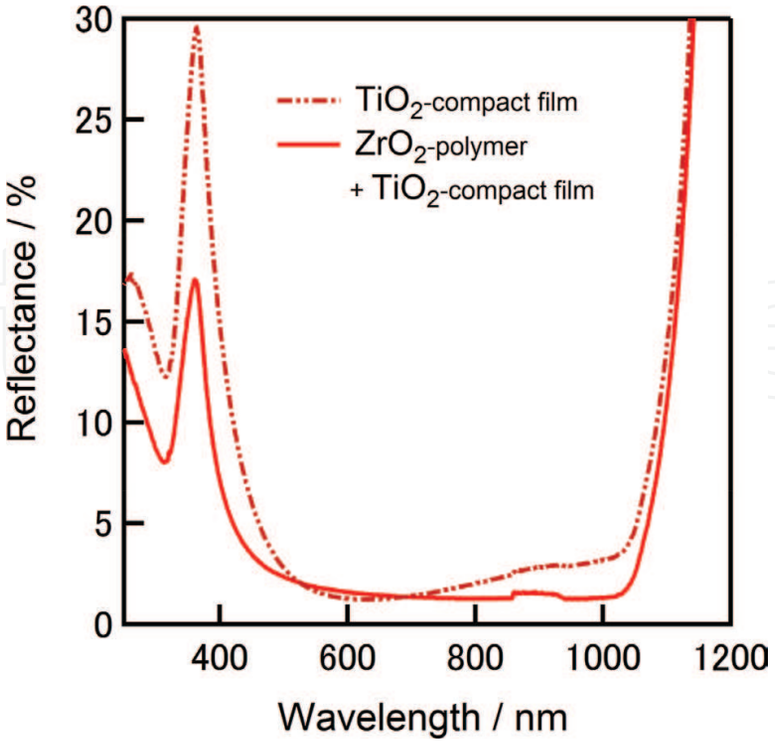

Figure 14. Comparison of the reflectivity of the textured silicon wafers with TiO_2 single layer and spin-coated ZrO_2/spray-deposited TiO_2 double-layer [17].

cells on with a single layer TiO_2-compact films on the wafer surfaces, ZrO_2-polymer composite films were deposited on the finished cells and compared to those of the cells without ARC and with single layer TiO_2-compact films. Deposition of ZrO_2-polymer composite ARC films were carried out by the annealing step after spin coating process (1000 rpm on flat surface, 1500 rpm on textured surface, 5 s acceleration+25 s, annealing at 125°C, 5 min).

Conversion efficiency of the cells improved from 15.2 to 15.9%, where the J_{sc} also increased further from 35.3 to 37.2 mA cm^{-2} owing to the ZrO_2/TiO_2 multilayer ARC film (the J_{sc} of the cell without ARC was 28.7 mA cm^{-2}). The electrical characteristics of the cells are summarized in **Table 4**.

A total of 70 mV increase of V_{oc} of the cells with ARC can be confirmed. Though, SiO_2 film was formed by thermal oxidation process at temperature of 800°C for 10 min under O_2 gas, the photovoltaic results with/without SiO_2 layer have not been compared in this study. Hence, the increase of V_{oc} is due to the compact TiO_2 layer, which can prevent excessive fire though of Ag into p-n junction. The greater *FF* of the cells with ARC layer can be attributed to the lower contact resistances in which the effect of additional SiO_2 layer can be considerable in order to avoid internal shunts. *J-V* characteristics of the silicon solar cells fabricated with TiO_2-compact single layer and ZrO_2-polymer composite/TiO_2-compact multilayer ARC on surface of the cells is given in **Figure 15**.

One can conclude that a significant improvement on J_{SC} and η could be confirmed owing to the ZrO_2-polymer composite/TiO_2-compact multilayer ARC when compared to the textured

http://dx.doi.org/10.5772/intechopen.68170

Surface structure	ARC	J_{sc} (mA cm^{-2})	V_{oc} (V)	*FF* (%)	R_{series} (Ω cm^2)	R_{shunt} (Ω cm^2)	η (%)
Textured	–	28.7	0.511	69.4	0.71	250	10.2
Textured	TiO_2-compact	35.3	0.581	74.1	0.40	655	15.2
Textured	ZrO_2-polymer/TiO_2-compact	37.2	0.583	73.4	0.45	535	15.9

Table 4. Photovoltaic characteristics of fabricated crystalline silicon solar cells with various surface structures with/without antireflection coating on textured surface [17].

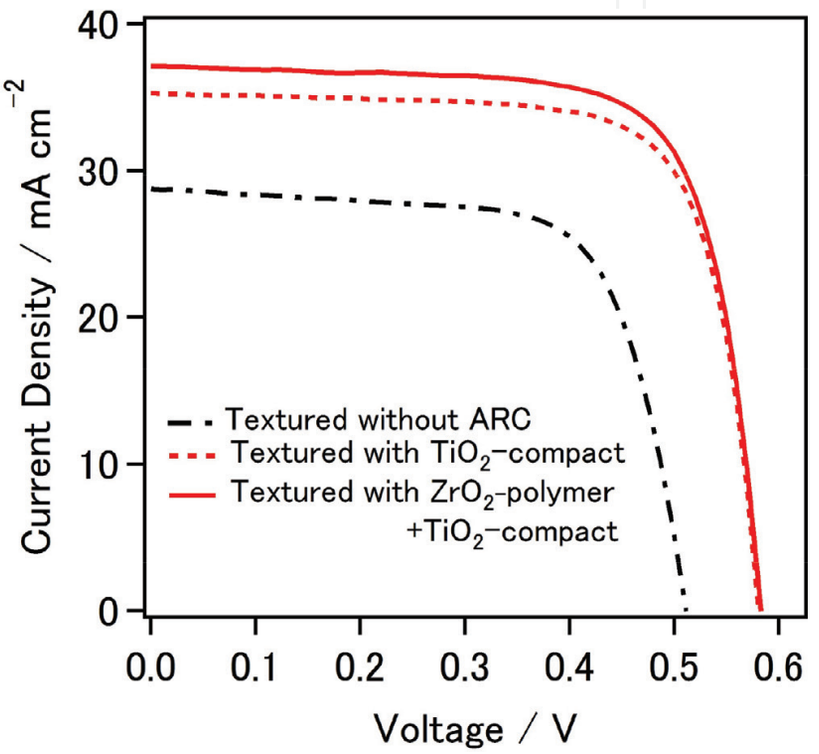

Figure 15. *J-V* characteristics of the silicon solar cells fabricated with TiO_2-compact single layer and ZrO_2-polymer composite/TiO_2 -compact multilayer ARC [17].

cells without ARC. The increase of the J_{SC} was related to minimizing the reflectance loses which can boost the performance of the cell. These results suggest that ZrO_2/TiO_2-based multilayer ARC films formed by spray pyrolysis deposition technique and spin coating technique could be an attractive alternative as a low-cost, simple, and vacuum-less process for ARC coating for silicon solar cells.

3.3. Spray deposited TiO_2 and Al_2O_3 films

3.3.1. Sample preparation

Compact TiO_2 and Al_2O_3 films formed by spray deposition technique are another attractive low cost ARC alternative for crystalline silicon solar cells. In this part, TiO_2 and Al_2O_3 film

formations on flat crystalline silicon substrates, evaluation of the coating films was carried out. And textured silicon solar cell fabrication with Al_2O_3/TiO_2 double-layer antireflection coating films was explained. The detailed analysis of the modeling to show the effects of organics can be found in Ref. [21]. For the experimental of optical studies, 25 × 25 mm^2 Cz-Si p-type wafers were used. All wafers were cleaned in 20% HF solution and soaked in ionized water. Then, UV/O_3 cleaning was applied in order to achieve a complete clean surface without mobile ions. Deposition of TiO_2 and Al_2O_3 films were established by spray pyrolysis. Prior to spraying process crystalline silicon wafers were set on a conventional hot plate and heated up until the surface temperature of the substrate reaches 450°C. The TiO_2 precursor solution was composed of titanium bis-isopropoxide bis-acetylacetonate (TAA) and ethanol (1:10%vl). The Al_2O_3 precursor solution was 0.03 M of aluminum (III) acetylacetonate ($Al(acac)_3$) in ethanol solution. Deposited film thicknesses were mainly controlled by the amount of sprayed precursor solutions. Each layer was analyzed by ellipsometer (Uvisel ErAgms-nds, Horiba Jobin Yvon).

3.3.2. Characterization of the films

At first, in order to analyze and optimize TiO_2 and Al_2O_3 spray on deposited layers for the processing of Al_2O_3/TiO_2 double-layer film, single-layer TiO_2 and Al_2O_3 films were analyzed. In depth analysis was carried out with fitting models of "flat layer" as the main body of the coated layer and "rough layer" as the surface residue when depositing a spray-deposited TiO_2 and Al_2O_3 films [21] and fitted according to the real SEM images. As an optimum value of 60 mL TiO_2 and 100 mL Al_2O_3 precursor solutions were considered. The analysis was carried out improved by considering the "void" and "organic" parts in the models. The existence of the organics and their contributions were confirmed by the FTIR measurements and by modeling [21]. For the optimization process of $\langle Al_2O_3/TiO_2 \rangle$ double-layer, thickness of TiO_2 film was varied between 20 and 120 nm (precursor solution 2–12 mL) while the thickness of Al_2O_3 film was changed from 68 to 135 nm (precursor solution 75–150 mL). After the reflectance measurements of the cells with ARC, the maximal short-circuit current densities from the reflectance results were calculated using Eq. (1) in order to observe the optimum Al_2O_3 and TiO_2 film thicknesses to obtain efficient Al_2O_3/TiO_2 double-layer ARC film.

Figure 16 presents the short-circuit current density ($J_{sc,max}$) calculated by (Eq. (1)) using experimental reflectance spectra of silicon substrate with Al_2O_3/TiO_2 ARC film for various thicknesses of Al_2O_3 and TiO_2 films. According to the calculations using experimental absorption spectra, the maximum value of short-circuit current density ($J_{sc,max}$) of 38.9 mA cm^{-2} was achieved with 90 nm Al_2O_3/40 nm TiO_2 double-layer ARC film (the data was not shown in the manuscript). Based on the experimental founding, 90 nm Al_2O_3/40 nm TiO_2 double-layer ARC film was applied when fabricating silicon solar cells which will be explained in following section. Comparison of reflectance of silicon surface with/without ARC and/or with/without texturing is given in **Figure 17**. As known texturing of silicon surface have a significant effect on reducing the reflectivity, as also proved in this study by the decrease of reflectance from 40 to around 20% after texturing. Considering the surface condition of a silicon substrate, reflectivity of 20.1 and 9.71% were observed on flat and

http://dx.doi.org/10.5772/intechopen.68170

textured surfaces, respectively. The effect of texturing on J_{SC} can be expected [22]. Owing to the double-layer ARC film the reflectivity was decreased down to the minimum of 0.4% at around 600 nm.

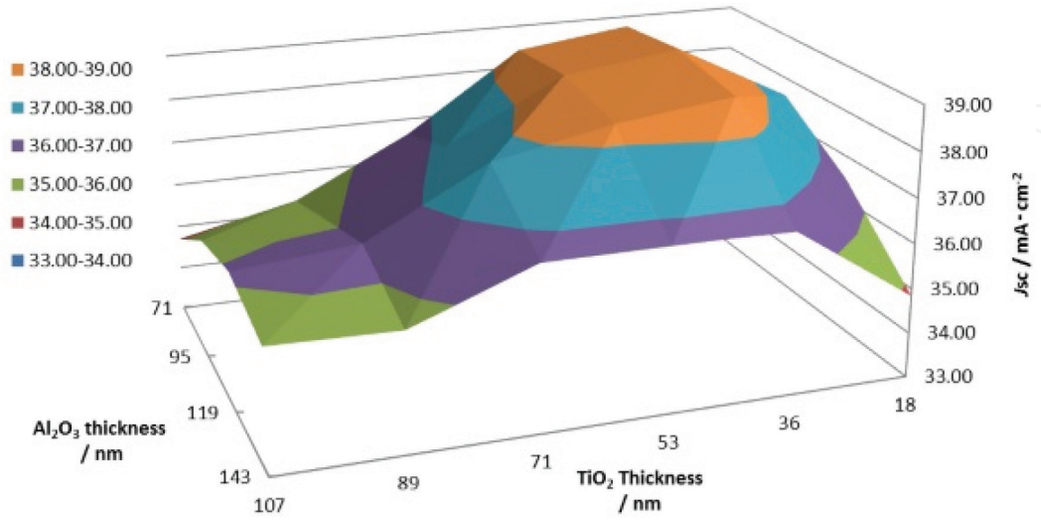

Figure 16. Estimated J_{sc} calculated by the experimental reflectivity data using $\langle Al_2O_3/TiO_2/Si\rangle$ layers with various thicknesses of Al_2O_3 and TiO_2 films [21].

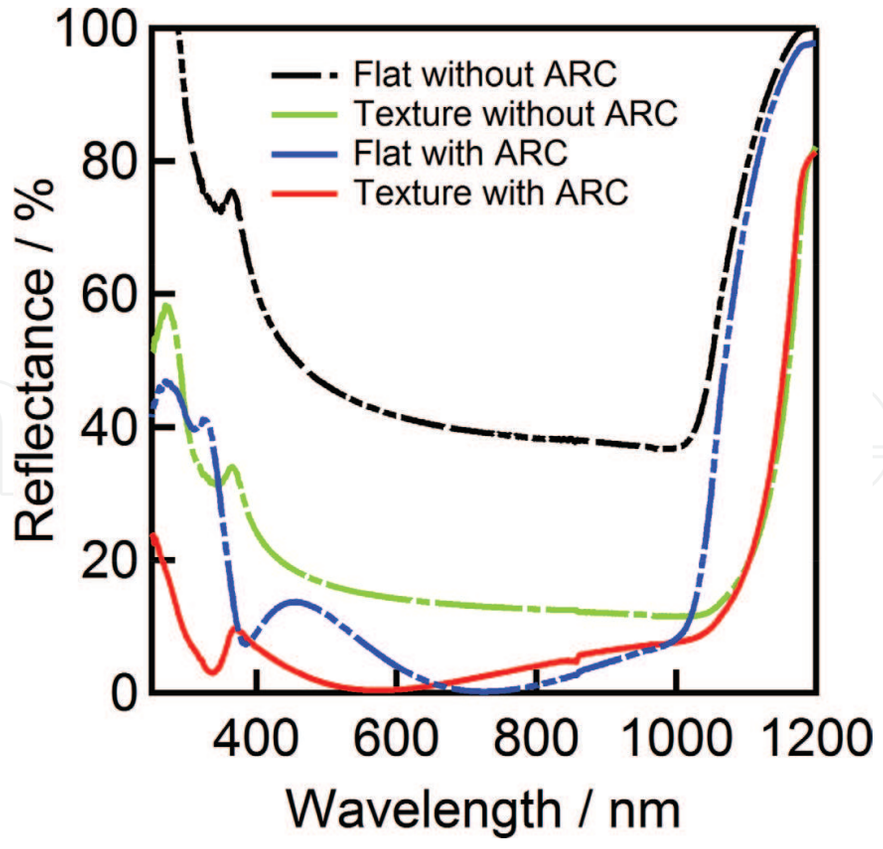

Figure 17. Reflectance spectra of silicon wafers with various surface structures [21].

3.3.3. Solar cell fabrication

Electrical characteristics of fabricated solar cells with various surface structure and ARC film were given in **Figure 18**, and summarized in **Table 5**. Comparing the flat or textured surface solar cells without ARC, J_{SC} of 27.6 mA cm^{-2} improved up to 33.5 mA cm^{-2} owing to the textured surface. In case of solar cells with Al_2O_3/TiO_2 double-layer ARC J_{SC} of solar cells were improved from 34.3 (flat surface) up to 37.0 mA cm^{-2} (textured surface). Consequently, the CZ-Si p-type solar cells with Al_2O_3/TiO_2 double-layer ARC on textured surface reached a η of 15.5% with a V_{oc} of 590 mV and *FF* of 71.2. A significant improvement on J_{SC} and η could be confirmed owing to the Al_2O_3/TiO_2 ARC when compared to the textured cells without ARC.

The ARC effect on the cells can be seen by the increase of J_{SC} (**Figure 18 (a)**) and can be confirmed by the EQE coverage over the spectrum (**Figure 18 (b)**). The suppression of EQE below 400 nm may be attributed to the absorption of TiO_2 layer. The ripples on EQE in the range of 500–1000 nm may take attention which is similar for all measurements at the same measurement points, can be considered as non-significant measurement errors. The decrease of open circuit voltage was attributed to the degradation of carrier lifetime of the bulk due to the over-annealing (>350°C) [23, 24]. In order to avoid this deterioration, an additional ultrathin passivation layer-like silicon dioxide may be formed between silicon substrate and TiO_2 layer to boost open circuit voltage. A J_{SC} calculation was performed for single layer of TiO_2 and SiN_x with theoretical reflectance and (Eq. (1)) which was resulted as 39.50 and 40.67 mA cm^{-2}, respectively. The J_{SC} of cells with TiO_2/Al_2O_3 double-layer ARC were estimated as 43.46 mA cm^{-2} which is above these values. In some references, also, the advantage of double-layer ARC was shown with low reflectance less than single layer ARC [25–28]. Moreover, another advantage of TiO_2/Al_2O_3 is the non-vacuum spray pyrolysis deposition, which can realize the

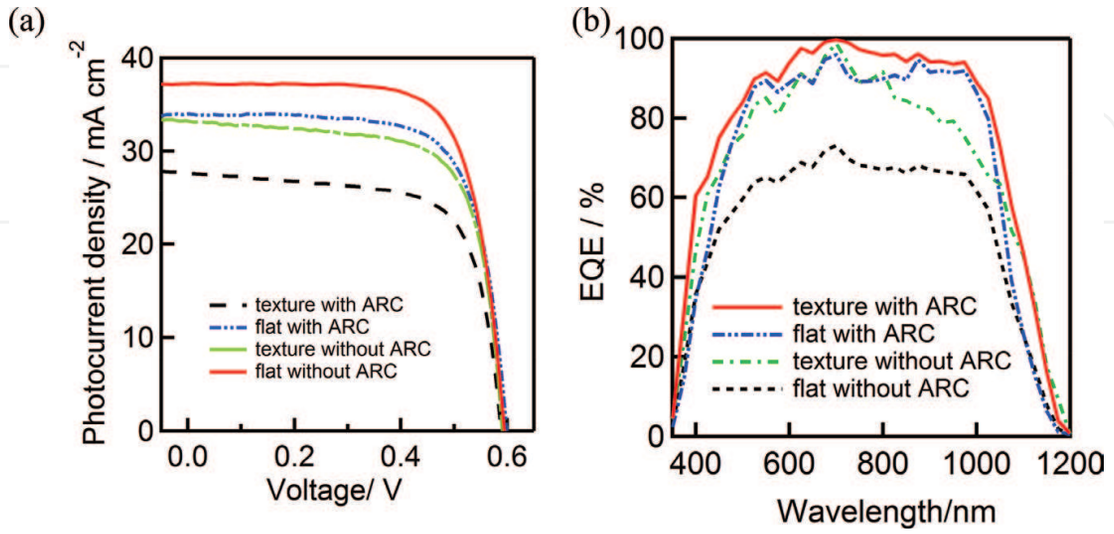

Figure 18. Current-voltage curves (a) external quantum efficiency (EQE) spectra and (b) of four fabricated sets of solar cells with/without texture and antireflection coatings (ARC) [21].

Surface structure	ARC	*Jsc*/mA cm^{-2}	V_{oc}/V	*FF*	η/%
Flat	Without	27.6 ± 0.1	0.588 ± 0.02	0.708 ± 0.012	11.5 ± 0.2
Flat	With	34.3 ± 0.8	0.596 ± 0.03	0.706 ± 0.014	14.4 ± 0.5
Textured	Without	33.5 ± 0.6	0.588 ± 0.05	0.702 ± 0.004	13.8 ± 0.2
Textured	With	37.0 ± 0.2	0.590 ± 0.09	0.712 ± 0.026	15.5 ± 0.8

The average data and the errors have been calculated using three different samples [21].

Table 5. Average data of photovoltaic characteristics of fabricated Si solar cells with various surface structures with/without surface texturing and antireflection coating (ARC).

lower cost production system than batch vacuum process like a SiN_x in terms of installation and running costs [29].

4. Screen-printing phosphorus diffusion for low-cost solar cells

A range of methods are in use to form n+ emitters or back surface fields for p-type silicon solar cells. Phosphorus oxychloride ($POCl_3$) is the main technique in the industry, while there are other alternatives as orthophosphoric acid (H_3PO_4) by spray or liquid sources by spin-on deposition techniques. Some have industrial application difficulties, high process cost, difficulty in wafers handling, or feasibility for batch or inline diffusion processes. Considering these techniques, screen-printing is a well-known and appealing technique with the advantages of low-cost, simplicity, both inline or batch mode diffusion possibility and industrial availability. In this study, screen-printing phosphorus diffusion is presented as an alternative to conventional dopant deposition techniques. Special attention was given to the impact of diffusion time, temperature variation, or the ambient gas effect during diffusion on the quality of screen-printed phosphorus diffusions on mc- and CZ-Si wafers. Diffusion tube with a gas input and output gates at the head and the end of the tube were used by changing the ambient during the diffusion process. By applying such a diffusion process we aimed to use the ambient effectively on diffusion process and adding to the diffusion time, diffusion temperature, the effect of ambient gas was also investigated.

4.1. Phosphorus oxychloride diffusion

Phosphorus diffusion using $POCl_3$ (phosphorus oxychloride) liquid source bubbled by N_2 is the dominant diffusion n+ emitter forming in silicon solar cell manufacturing process. Overall diffusion process occurs in two main steps: predeposition and drive-in. During predeposition, liquid $POCl_3$ source bubbled by N_2 gas flow and, evaporated source go through the chamber to react externally introduced O_2. This reaction takes place according to Eq. (2) in order to form P_2O_5 on the surface of wafers while Cl_2 is aired out during the reaction. The schematics of the $POCl_3$ diffusion process can be seen in **Figure 19**.

$$4\,POCl_3 + 3\,O_2 \rightarrow 2\,P_2O_5 + 6\,Cl_2 \quad (2)$$

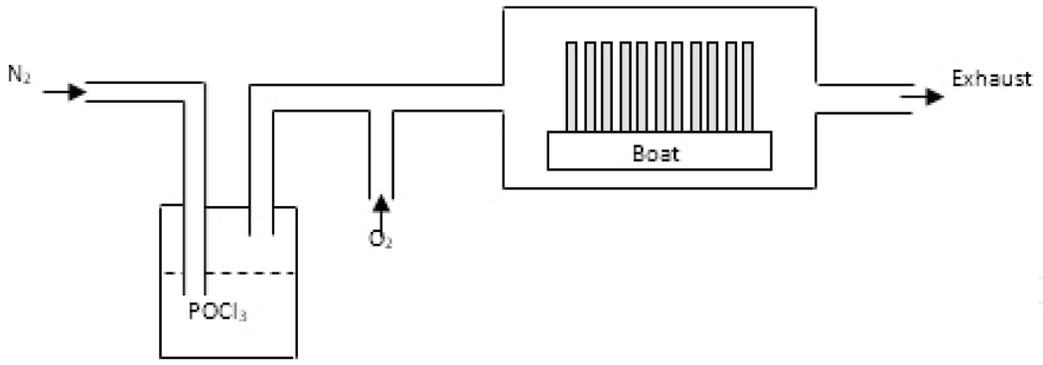

Figure 19. The schematic of $POCl_3$ diffusion system.

After predeposition step, $POCl_3$ source is halted and drive-in process starts to take place via the deposited phosphorus rich layer on the surface. During the drive-in step, diffusion of phosphorus atoms into silicon occurs through the reduction of P_2O_5 by silicon according to Eq. (3).

$$2\,P_2O_5 + 5Si \rightarrow 5\,SiO_2 + 4P \tag{3}$$

Generally, predeposition step is applied at lower temperatures than the drive-in step where the formation of diffused phosphorus layer establishes when the drive-in comes up. The surface concentration of diffused layer is controlled by increasing the O_2 gas flow during the drive-in process.

In silicon solar cell manufacturing process, wafers are stacked vertically in a boat in a furnace as in **Figure 19** prior to $POCl_3$ diffusion. If the wafers are set in order one by one, both side of wafers achieved similar diffusion of phosphorus. By that, gettering of impurities in silicon can also accomplish owing to the advantage of two side diffusion. However, back-to-back setting order also widely used for manufacturing in order to diffuse as much samples in a single process. One of the disadvantages of the $POCl_3$ diffusion system is that the same amount of source has to be used even for small size wafers because of the batch nature of the system. Additionally, long ramp-up and ramp-down cycles may be required which leads to time consumption even though the independent control of the predeposition and drive-in steps is an advantage.

4.2. Screen-printing phosphorus diffusion

As explained under Section 2.2, screen-printing is a fast, reliable and cost effective technology which is mainly used for metallization purposes for silicon solar cell industry. Screen-printable dopant sources are also introduced to the photovoltaic industry and are under research. As an attractive technology to deposit dopant sources on the surface of the substrates makes inline diffusion process possible to form dopant-diffused layers. After the deposition, diffusion process is usually performed by using either belt furnaces or quartz tube at high temperatures. Applied dopant paste usually is needed to be dried before the thermal annealing. Similarly, to the other diffusion techniques, after the deposition of the dopant paste by screen-printing, phosphorus atoms are released from the dried paste during the diffusion according to reduction of P_2O_5, as

given in Eq. (3). Among other advantages, the availability to form homogenously diffused layers, the possibility of forming selective structures in any desired pattern are some of the most attractive points of using screen-printing technique dopant diffusion.

4.3. Diffusion process equipment

Both for solar cell manufacturing in industry or research and development of dopant diffusion process are mainly performed by using quartz tube or belt furnaces. A brief introduction of each equipment and technique will be given.

4.3.1. Diffusion in quartz tube

For diffusion process in quartz tube, wafers are set to a loading boat and are placed in the quartz tube. Diffusion process takes place according to the settled thermal cycle profile. The scheme of the quartz tube and heating system is given in **Figure 20**. The ambient inside the tube can be varied by changing the gas introduced into the tube from the end-side of the tube. Diffusion by solid sources of for $POCl_3$ and BBr_3 bubbled by N_2 needs to be carried out by such a tube. For other deposition techniques including screen-printing, spin-on, or spray deposition, it is possible to diffuse wafers from a single side or both sides. Depending on the type of quartz tube, gas ambient inside the tube can be controlled by introducing more than one gas separately.

4.3.2. Diffusion in belt furnace

Diffusion by a belt furnace offers a fast ramp-up and cool-down processes usually by infrared heating systems which can shorten the total process time significantly. These kinds of systems usually have a couple of separated heating zones. The control of the diffusion profile is usually carried out by setting different temperatures for each zone and by the speed of the belt. Also, gases can be introduced through the openings to change the ambient. Single or double side diffusion is both possible for belt furnace diffusion. For single-side diffusion, SOD method, spraying, or screen-printing technique are usually used. The most important drawback of belt furnace diffusion is the contamination by metallic impurities due to the conveyer belt.

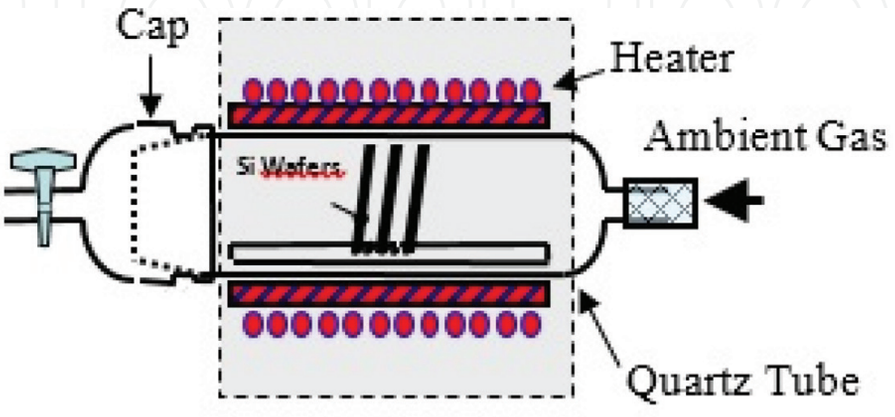

Figure 20. Quartz tube diffusion system.

5. Screen-printing phosphorus diffusion on P-type c-Si

5.1. Sample preparation and experimental

A total of 1.2 Ωcm mc-Si and 2.5–3 Ωcm CZ-Si p-type wafers with a surface area of 50 × 50 mm^2 were used for the quality evaluation experiments of the screen-printing phosphorus diffusion using Aquanyl phosphorus source provided by Nippon Gohsei Co. For the texturing of mc-Si p-type wafers, HF: HNO_3 (1:10 vl%) was used. CZ-Si p-type wafers were alkaline textured in KOH bath at 80°C. After printing the phosphorus paste on both side of the wafers by a screen-printing machine, wafers were dried at 150°C for 3 min. Diffusion process was carried out in a conventional quartz tube furnace in various ambients (Ar, N_2, O_2, and N_2+5% O_2) at peak temperatures of 875 and 900°C. For the sheet resistance evaluation, phosphorus silica glass was removed first by 5% HF and sheet resistances were measured by four-point-probe method. In case of lifetime studies, $n^+/p/n^+$ symmetric structures were formed on mc- and CZ p-type wafers and the effect of impurity gettering was evaluated after phosphorus diffusion. In order to estimate the carrier lifetime of the bulk, n+ layers were etched away using HF:HNO_3 (1:10 vl%) and minority carrier lifetimes were measured using the QSSPC [31, 32] technique after 3% iodine-ethanol chemical passivation.

5.2. Impact on sheet resistance

Diffused layers are basically characterized by sheet resistance, R_{sheet}, which is the ratio of resistivity, ρ, to thickness of the sample, d, $R_{sheet} = \rho / d$. In this study, ambient gas, diffusion temperature and the diffusion time are important parameters that affect the value of sheet resistance after diffusion. In order to minimize front recombination losses high sheet resistances are advantageous for n^+ emitter crystalline silicon solar cells. However, high sheet resistances limit to obtain a good Ω contact for metallization. On the other hand, these recombination losses can be reduced by lowering the phosphorus concentration which can lead an enhancement of blue response and thus the efficiency of solar cells.

Figure 21 shows the effect of the sheet resistance of emitter on internal quantum efficiency (IQE) in short wavelength range simulated by PC-1D. As can be seen, the higher the sheet resistance emitter, the better the blue response. High-efficiency devices using lithography or any advanced metallization contact technology can use high sheet resistance emitter potential. In case of $POCl_3$ diffusion, the control of sheet resistance is managed by temperature profile and diffusion ambient [33]. In this work, screen-printing phosphorus diffusion was carried out at peak temperature of 875 and 900°C in different ambients. **Figure 22** shows the average sheet resistances of phosphorus-diffused mc- and CZ-Si p-type wafers for each diffusion condition. For the mc- and CZ-Si p-type wafers sheet resistances of phosphorus diffused at 875°C in Ar, N_2, and N_2 + 5% O_2 ambient resulted in a range of from 80 to 90 and from 60 to 70 Ω sq^{-1}, respectively. At the peak diffusion temperature of 900°C, the range of sheet resistances were from 40 to 50 and from 30 to 40 Ω sq^{-1}, for mc and CZ-Si wafers, respectively.

Higher sheet resistances were observed at both 875 and 900°C in ambient O_2 for both types of wafers. The phenomenon of diffusion of screen-printed phosphorus into the silicon wafers can be explained by the reduction reaction of P_2O_5 with silicon as in Eq. (3). Surface of the

http://dx.doi.org/10.5772/intechopen.68170

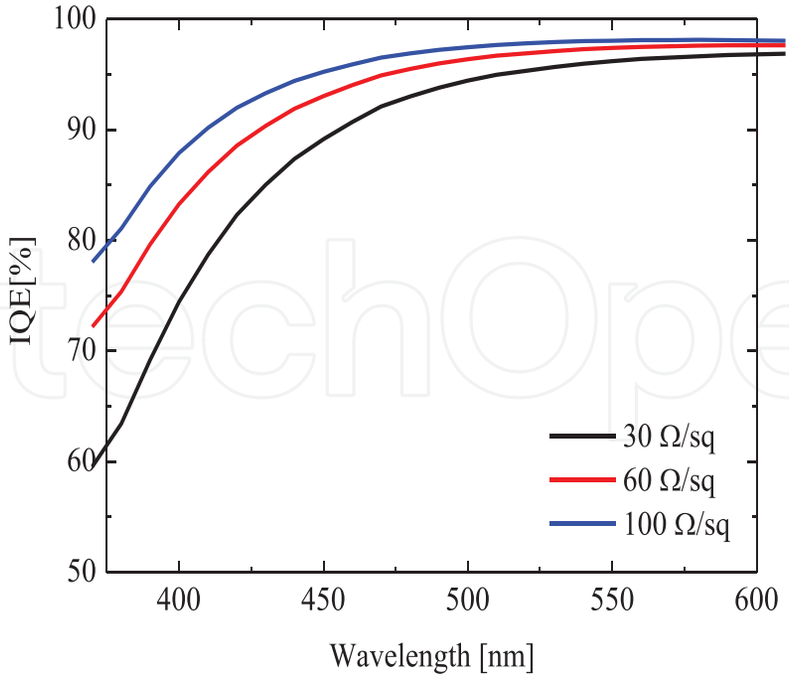

Figure 21. The simulated internal quantum efficiency (IQE) for different sheet resistances by PC-1D.

silicon oxidies are faster with the existence of O_2 ambient. Due to the heavy O_2 flow during the diffusion may cause reoxidation of phosphorus atoms. Thus, limits the amount of phosphorus atoms to be diffused which results high sheet resistance [30]. As a conclusion of that, 100% O_2 ambient may not be suitable for quality emitter formation. These results shows that proper emitter sheet resistances can be controlled by adjusting the diffusion temperature, diffusion time, and ambient gas in a similar manner as in the $POCl_3$ diffusion process when adapting a proper screen-printing dopant paste.

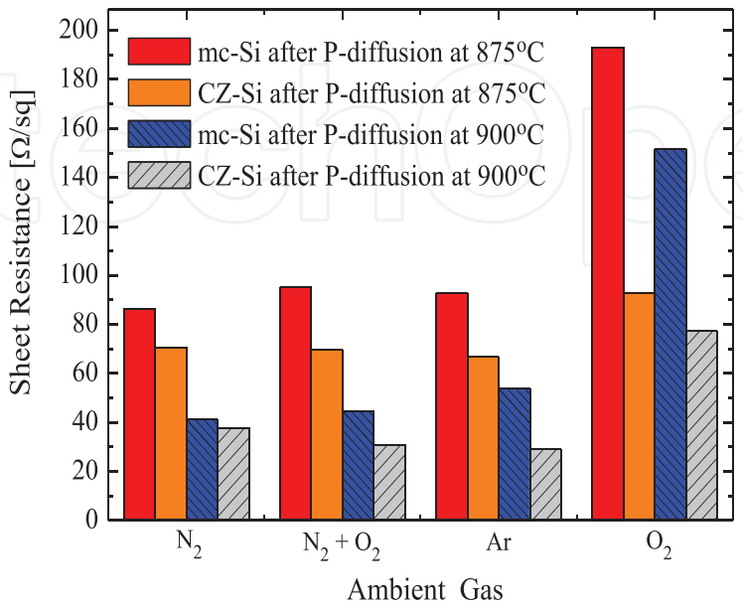

Figure 22. Sheet resistances measured on mc- and CZ-Si wafers after phosphorus diffusion at 875 and 900°C for 30 min [30].

5.3. Impact on carrier lifetime improvement

Metallic impurities have a lifetime killing effect for crystalline silicon solar cells, which becomes more crucial especially when using low solar grade silicon to grow mc-Si ingots. Especially top and bottom of the ingots contains high concentrations of metal impurities [34], which requires additional gettering before or during solar cell processing [35]. It is well known that the detrimental effect of these impurities can be reduced by can be reduced by phosphorus gettering [36, 37]. Owing to the phosphorus gettering, bulk lifetime of the silicon wafers can be improved by removing the impurities. In this work, $n^+/p/n^+$ symmetric structure of mc- and CZ-Si p-type wafers were formed by phosphorus diffusion in order to examine the effect of phosphorus gettering for our screen-printing diffusion process via estimation of bulk lifetimes. As a reference, initial lifetimes of the wafers were measured prior to phosphorus diffusion after removing the saw damages by acidic etching and then by using chemical passivation with a 3% iodine–ethanol solution for the measurement. These initial lifetimes were compared by post diffusion lifetimes after removing n^+ layers by acidic etching and passivating the bulk by the 3% iodine–ethanol chemical passivation as that used for the initial lifetime measurements. **Figure 23 (a)** and **(b)** shows the average carrier lifetime dependence of CZ and mc-Si p-type wafers to the ambient gas and diffusion temperature. After diffusion in ambient N_2, N_2+5%O_2, and Ar, improvement of carrier lifetimes were observed for both type of wafers. After diffusion at 900°C in ambient N_2, carrier lifetimes of CZ-Si p-type wafers reaches up to 350 μs from initial value of 200 μs [30].

The carrier lifetimes of mc-Si p-type wafers increased to up to 70 μs, about a tenfold increase from the initial carrier lifetime, as given in **Figure 23 (b)**. Considering that all wafers went through the same procedures before and after the diffusion processes, carrier lifetime improvements can be attributed to the gettering effect. The effect of oxygen on carrier lifetime was clearer for mc-Si wafers that show a good gettering effect even for shallow emitters.

The excess carrier dependent lifetimes for the CZ and mc-Si wafers improved and higher carrier lifetimes were realized at low-injection levels after phosphorus diffusion as shown in **Figure 24 (a)** and **(b)**.

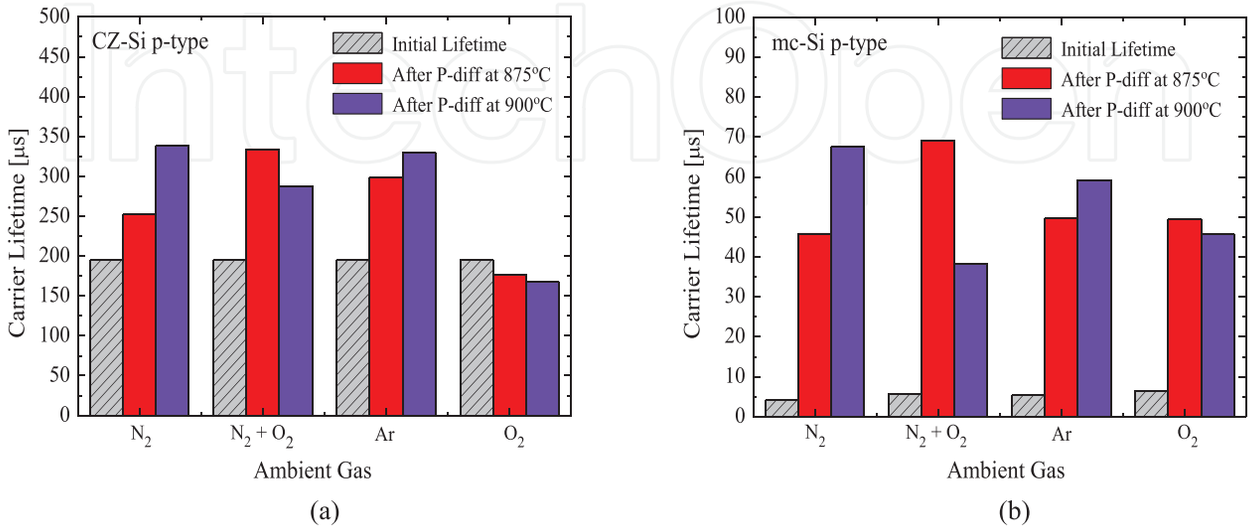

Figure 23. Increase in carrier lifetime after phosphorus diffusion on (a) CZ-Si wafers and (b) mc-Si wafers at different temperatures and in various ambient gases [30].

http://dx.doi.org/10.5772/intechopen.68170

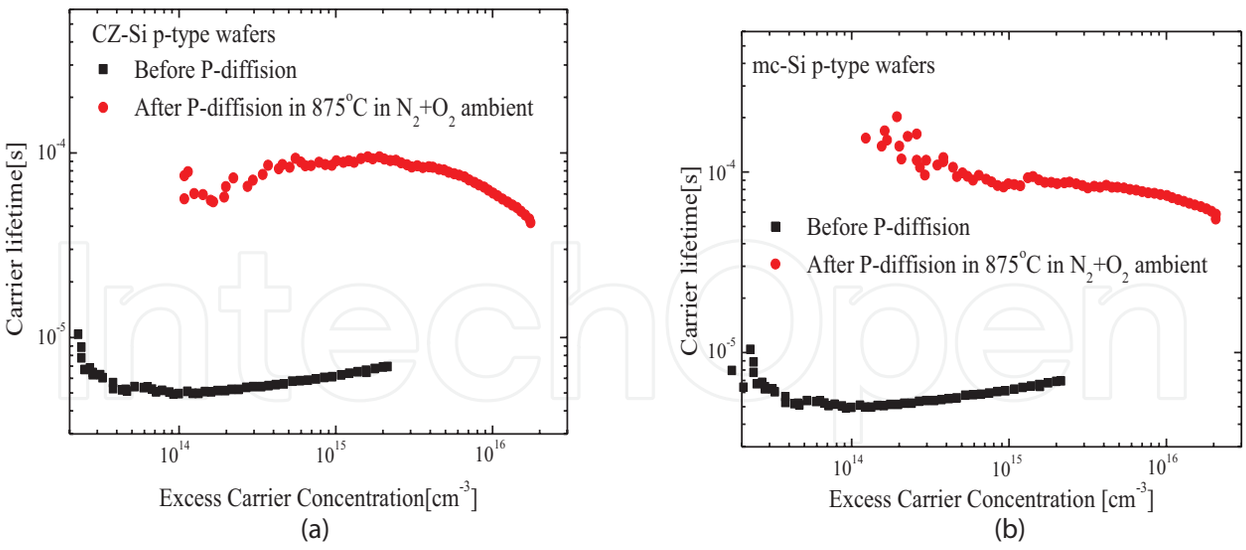

Figure 24. The carrier lifetime as a function of excess carrier concentration in (a) CZ-Si wafers and (b) mc-Si wafer before and after phosphorus diffusion [38].

6. Selectively screen-printing and single diffusion process

A lowly doped shallow emitter is required for a good blue response and a high quantum yield [39, 40]. However, a highly doped deep emitter is required for a good Ω contact for metallization. A selective emitter structure is an optimum tradeoff to combine these both emitter conditions with highly doped low sheet resistance regions under the printed contact fingers and lowly doped high sheet resistance regions between the fingers [41]. By the advantage of that, selective structures lower the surface recombination velocity of minority carriers [42], and leads to reduced contact series resistances as well [43, 44]. Additionally, blue response of solar cells can be improved [45, 46], high open circuit voltage and fill factor [47] can be achieved owing to the selective emitter structures. There are various techniques and applications to form selective emitter structures [48]. Double-diffusion with masking [49, 50], selective diffusion barrier process [51], oxide masking process and etch back [45, 52], implantation process [53] are among these techniques. Depending on the technique, need of laser ablation, additional steps like masking, repeated diffusions, etch back processes are among the drawbacks of such techniques. A screen-printable ink based on Si-nanoparticles was also provided which are selectively deposited prior to phosphorus diffusion to form heavily doped areas of the selective emitter structure [54]. This technology is already commercially available and includes an extra step of diffusion process for mass production. For instance, in laser doping through PSG [55], a light $POCl_3$ diffusion is performed first and resulted PSG acts as a doping source and highly doped regions are formed by laser ablation. Another laser-based process [47] offers a formation of the passivation layer simultaneously with structuring a highly doped region by a laser beam processing. There can be find some other processes for selective emitter solar cells mostly at research levels [56–59]. On the other hand, as a simple process for the formation of selective structures with single diffusion [60], based on the auto-diffusion mechanism, highly and lowly doped regions are formed at a single diffusion step. In this work, a single diffusion screen-printable diffusion technique is discussed as a simple and cost-effective method for industrial

selective emitter cell processing. Applicability of forming selectively diffused structures using screen-printing phosphorus paste on p-type mc-Si and CZ-Si wafers will be explained.

6.1. Sample preparation and experimental

A total of 50 × 50 mm^2 alkaline-textured CZ- and acid-textured mc-Si p-type wafers were used for the characterization. Phosphorus diffusion paste was selectively screen-printed on the surface of the wafers using a 200 μm finger pattern and dried for 3 min at 150°C. Phosphorus diffusion was performed in a conventional furnace for 30 min at a peak temperature of 875°C in N_2+5%O_2 ambient. After phosphorus diffusion, PSG glass and oxide layers were removed by 5% HF and the selective emitter sheet resistance was determined using the specially optimized four-point-probe machine to estimate the sheet resistance of the selective emitter structures. Since phosphorus dopant paste was screen-printed selectively on CZ- and mc-Si p-type wafers with the same pattern as metal contacts, beneath the screen-printed phosphorus lines, the silicon wafer was doped heavily. The regions between the lines were doped lightly by doping atoms diffusion from the printed source via the gas atmosphere. **Figure 25** shows the principle of single screen-printing phosphorus diffusion to form the selective emitter structure.

6.2. Sheet resistances of selective emitter structure

In order to confirm that this simple process ability to form selective emitter structures, sheet resistances of CZ, and mc-Si p-type wafers were measured after diffusion of selectively printed phosphorus source. To examine the pattern of the formed selective emitter, a line scan was performed by four-point-probe measurements. The distribution of measured sheet resistance after the phosphorus diffusion for 30 min at 875°C in N_2+5%O_2 ambient on selectively screen-printed CZ-Si p-type substrates is shown in **Figure 26**.

Lower sheet resistance under the printed fingers and higher sheet resistance between the fingers can be confirmed. It should be noted that the accurate values of sheet resistances of the structure may differ from these measured values due to tight geometry of the selective emitter structure which can affect the measurement. However, highly diffused regions beneath the printed area and shallow regions between the printed areas can still be confirmed after the single screen-printed phosphorus diffusion process. One can conclude selective emitter structure can

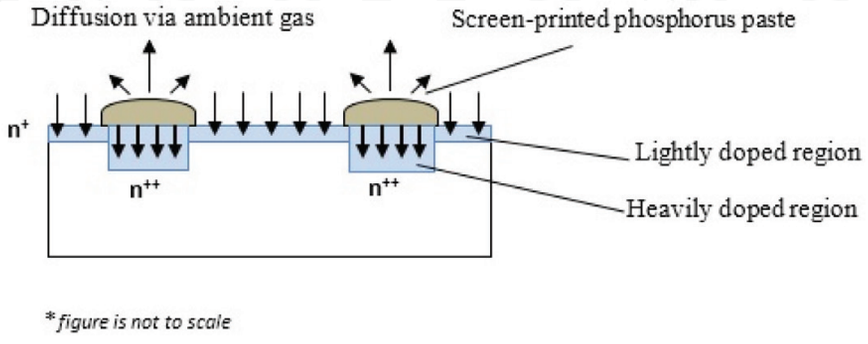

Figure 25. Principle of selective emitter formation process by single screen-printed phosphorus diffusion [30].

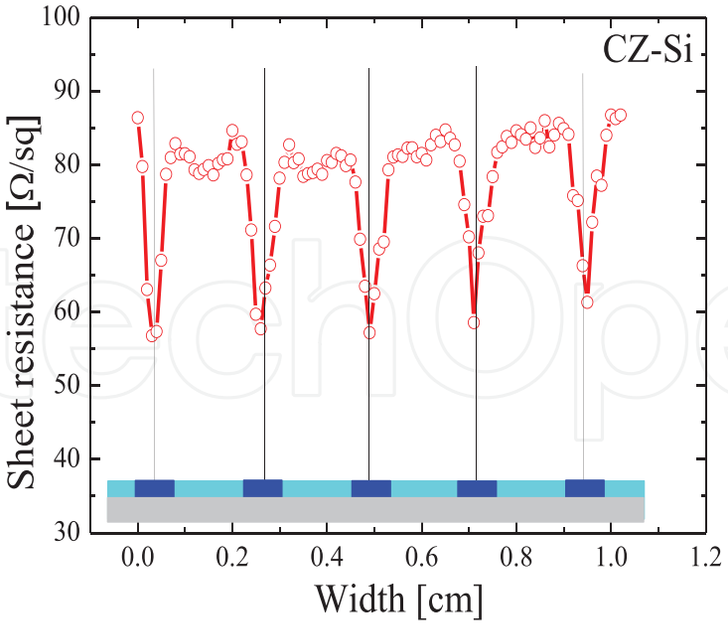

Figure 26. The distribution of measured sheet resistance after the phosphorus diffusion on selectively screen-printed CZ-Si p-type wafer [30].

be achieved with a single diffusion of a screen-printing phosphorus diffusion paste taking the advantage of auto-diffusion. Shallow regions under the illuminated area make it possible to have a better current collection properties and a low dark saturation current can be achieved by proper passivation applications [61, 62]. In order to confirm the diffusion profile of selectively screen-printed phosphorus, secondary ion mass spectrometry (SIMS) analysis was performed [30]. **Figure 27** shows SIMS profiles measured at two different region; under the printed finger area (highly doped region) and between the printed fingers (lowly doped region) of a CZ-Si p-type wafer went under single phosphorus diffusion process (875°C for 30 min in N_2+5%O_2 ambient).

Surface dopant concentration of the finger area was realized as a value of 1.4×10^{21} cm^{-3} and the concentration of the area between the fingers was realized as a lower value of 4.7×10^{20} cm^{-3} which shows the effect of auto-diffusion to achieve selective emitter structure. The actual sheet resistances were calculated using the SIMS data and estimated as 15 and 45 Ω sq^{-1}, under and between the fingers, respectively.

The sheet resistances base on the SIMS profile were calculated as follows; in order to calculate the carrier mobility first, μ_{max} and μ_{min} were set to 1414 and 68.5 cm^2 Vs^{-1}, respectively. N_0 was 9.2×10^{16} cm^{-3} and absorption coefficient α is set as 0.711 and N is the actual concentration taken from the SIMS measurement. Mobility of carriers was calculated according to Eq. (4).

$$\mu_n = \mu_{min} + \frac{(\mu_{max} + \mu_{min})}{1 + \left(\frac{N}{N_0}\right)^{\alpha}} \tag{4}$$

After determination of the carrier mobility, resistivity was calculated using Eq. (5).

$$\rho = \frac{1}{qN\mu_n} \tag{5}$$

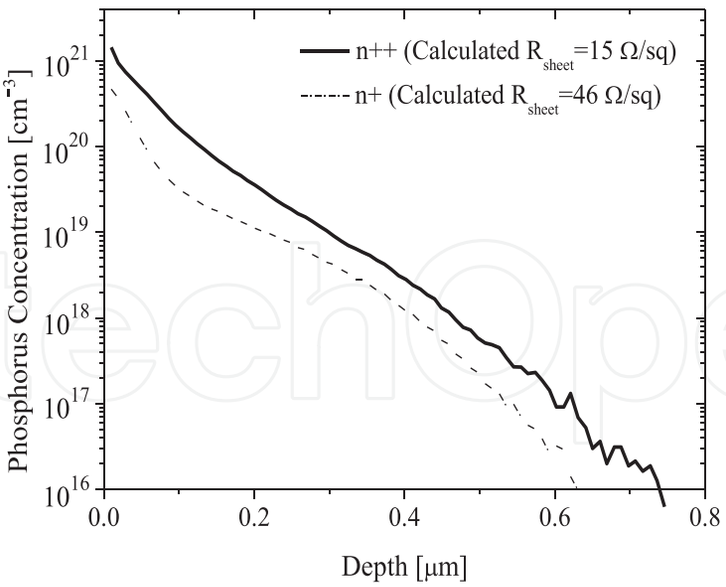

Figure 27. SIMS profile of highly doped regions under the fingers and lowly auto-doped regions between the fingers diffused at 875°C for 30 min [30].

Sheet resistance was calculated per each layer according to the following Eq. (6).

$$R_{shpl} = \frac{\rho_1 + \rho_2}{2(x_2 - x_1)} \tag{6}$$

Finally, total sheet resistance was calculated as the sum of inverse values of the sheet resistances per layer, as defined in Eq. (7).

$$R_{sh \cdot total} = \sum (R_{shpl})^{-1} \tag{7}$$

7. Single diffusion selective emitter solar cell fabrication

7.1. Sample preparations and experimental

Industrial-type selective emitter monocrystalline silicon solar cells with area of 156 × 156 mm^2 were fabricated by the single screen-printed diffusion process and compared to the homogenous emitter solar cells fabricated with standard $POCl_3$ diffusion. The process sequence used in this experiment is shown in **Figure 28 (a)**.

The screen-printing patterns of the printed dopant paste and the metal fingers as in **Figure 28 (b)** were similar in shape. However, the width of the fingers of printed paste was wider than the width of the metal finger to ensure the alignment. In case of the fabricated solar cells, the width of the phosphorus printed fingers were 400 μm where the finger width of the metal contacts was 70 μm.

Figure 29 shows the SIMS profiles of the selective structure formed on a CZ-Si p-type by single phosphorus diffusion at optimized conditions for the cell fabrication process at 870°C for 10 min in ambient N_2+5%O_2. However, note that the SIMS analyses of carbon, oxygen, and phosphorus concentrations were measured in cycles 10 nm, where the first 20 nm were used

http://dx.doi.org/10.5772/intechopen.68170

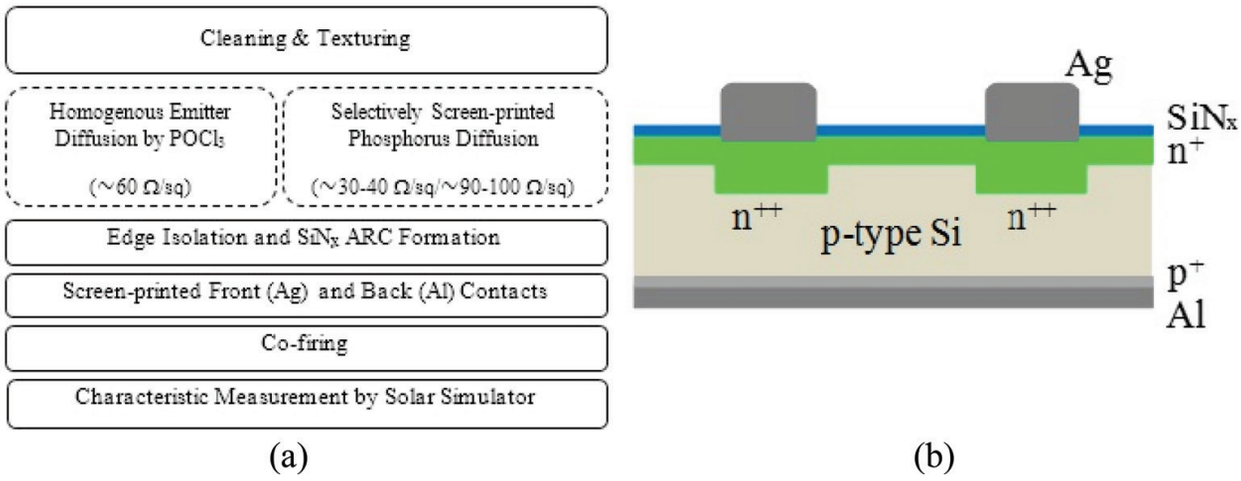

Figure 28. (a) Process sequence of cell fabrication process and (b) schematic of selective emitter solar cell with highly doped regions under the contacts and lowly doped regions between the contacts.

for the carbon and oxygen analyses and the phosphorus was measured starting from the 30 nm cycle. Therefore, the data of the first 20 nm depth was not obtained, and the actual surface concentrations are higher than the maximum values shown in **Figure 29**.

7.2. Fabricated homogenous and selective emitter solar cells

Table 6 summarizes the I–V measurement results of the homogenous emitter and selective emitter solar cells as measured by a calibrated solar simulator: the short-circuit current densities (J_{sc}), open-circuit voltages (V_{oc}), fill factor (*FF*), and conversion efficiency (*Eff*).

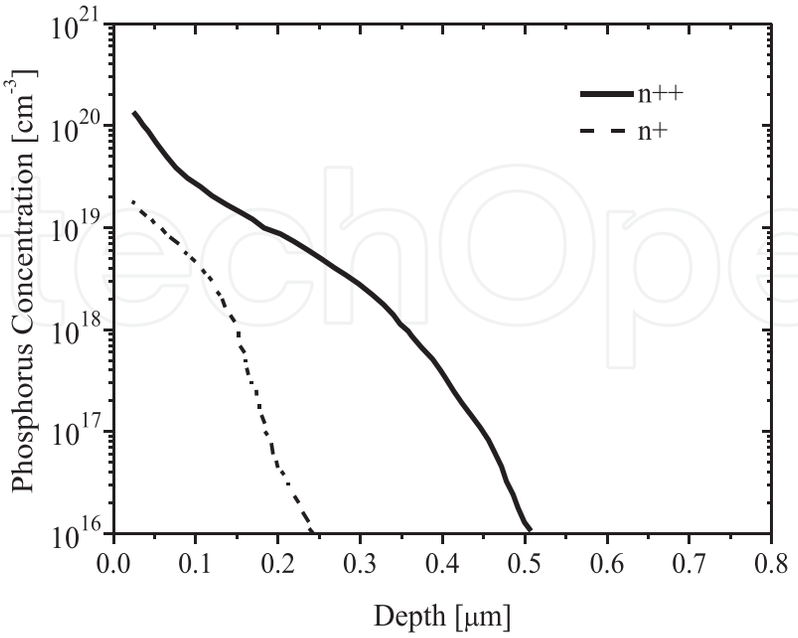

Figure 29. SIMS profiles of highly doped regions under the contacts and out-diffused lowly doped regions between the contacts diffused with the similar profile used for solar cell fabrication at 870°C for 10 min.

		V_{oc} (mV)	J_{sc} ($mAcm^{-2}$)	*FF* (%)	*Eff* (%)	I_{sc} (A)	V_{pm} (mV)	I_{pm} (A)	P_{max} (W)	R_s (Ωcm²)	R_{sh} (Ωcm²)
Homog. emit.	Avg.	618	36.4	77.9	17.5	8.7	518	8.1	4.2	1.1	3250
	Best	**617**	**36.6**	**78.3**	**17.7**	**8.7**	**518**	**8.2**	**4.2**	**1.1**	**2440**
Select. emit.	Avg.	625	36.3	79.2	17.9	8.7	528	8.1	4.3	1.1	5020
	Best	**625**	**36.5**	**79.2**	**18.1**	**8.7**	**529**	**8.2**	**4.3**	**1.0**	**21,700**

Table 6. Electrical characteristics of homogenous emitter and selective emitter solar cells [30].

The improvements in V_{oc} and *FF* by the selective emitter structure were confirmed. As shown in **Table 6**, the V_{oc} of the selective emitter cells was clearly improved by about 7 mV. The *FF* of selective emitter solar cells all exceeded 79%, which is an average increase of 1–2% compared to the homogenous emitter solar cells. However, no clear improvement in the short-circuit current was observed. The short-circuit currents seem to have been limited by the higher carrier recombination velocity due to the larger finger widths of the phosphorus-dopant paste and/or lower surface passivation effects. If surface passivation can be further improved, higher *FF* and V_{oc} can be also realized owing to the reduced defects and carrier recombination in the emitter region [63]. Thinner finger widths of phosphorus dopant paste can be considered to enhance current collection on the surface.

Figure 30 shows a comparison of the I–V curves of the best homogenous emitter solar cell and selective emitter solar cell. These results demonstrate the first trial of selective emitter formation using our screen-printed phosphorus source to prove the validity of the concept of single diffusion process. Further optimizations are in progress to realize higher efficiencies.

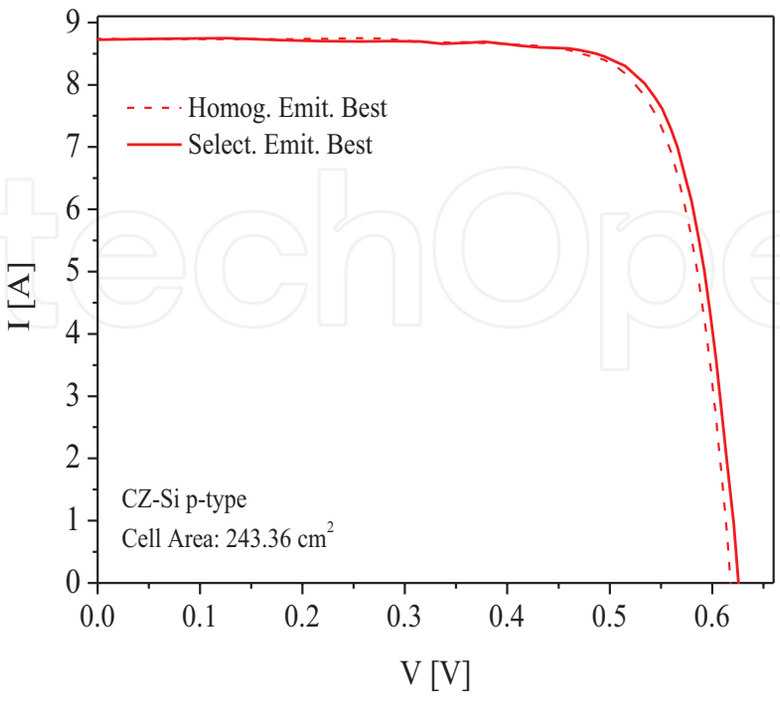

Figure 30. *I-V* curve comparison of the best homogenous emitter and selective emitter solar cells [30].

http://dx.doi.org/10.5772/intechopen.68170

8. Conclusion

Non-vacuum processing techniques for cost-effective and simple crystalline silicon solar cell manufacturing were introduced. A special attention was given to the low-cost spin coating and spray deposited ARC alternatives instead of the main stream SiN_x ARC and to the low-cost screen-printing phosphorus doping process with the application of selective emitter solar cells accomplished by a single deposition and single diffusion step. About the introduced materials and films, first evaluation of the material and processes were carried out and then silicon solar cells were fabricated. ZrO_2-polymer composite/surface-deactivated TiO_2-polymer composite films were introduced by spin coating deposition method and best efficiency of 12.91% was achieved with *J*sc of 31.42 mA cm^{-2}, V_{oc} of 575 mV, and fill factor *(FF)* of 71.5%. An improvement of 0.86% with an increase of *J*sc of 2.07 mA cm^{-2} was confirmed when compared to those of fabricated cells without the ARC. TiO_2-compact and ZrO_2-polymer composite antireflection coating layers were also introduced by simple and cost-effective spray pyrolysis deposition and spin coating process. Decrease in surface reflectance below 2% was confirmed owing to the ZrO_2-polymer composite/TiO_2-compact multilayers from around 550 –1050 nm of the spectrum. Efficiency of the fabricated cells increased up by a factor of 0.8% and reaches 15.9% with further increase of *J*sc 2 mA cm^{-2} owing to the applied ZrO_2-polymer composite/TiO_2-compact multilayer ARC. In case of spray pyrolysis deposition-based Al_2O_3/TiO_2 double-layer ARC, a reflectivity lower than 0.4% could be confirmed at 600 nm. Average conversion efficiency of fabricated cells (average of four samples) were 15.5% with a J_{SC} of 37.0 mA cm^{-2}, where the improvement was about 3.5 mA cm^{-2} and 1.7% on J_{SC} and on efficiency, respectively. Considering the future lowcost solar cells with non-vacuum process, introduced ARC films with good optical properties can be a promising alternative for ARC of solar cells. On the other hand, a cost effective screen-printing phosphorus diffusion process was introduced for an easy forming of selective emitter solar cells. Owing to the phosphorus diffusion carrier lifetimes of CZ-Si p-type wafers could be improved from 195 up to 350 μs through phosphorus gettering. By a single print and single diffusion process lowly and highly doped regions were achieved for selective emitter solar cell applications. Large-area monocrystalline solar cells were fabricated successfully by this method and more than 18% conversion efficiency was achieved. As an attractive and cost effective method, adapting such simple methods including spin coating, spray deposition, or screen-printing methods to all solar cell manufacturing sequences are believed to be play a key role for future low-cost solar cells.

Author details

Abdullah Uzum[1,2], Seigo Ito[1]*, Marwan Dhamrin[3] and Koichi Kamisako[3]

Address all correspondence to: itou@eng.u-hyogo.ac.jp

1 University of Hyogo, Himeji, Japan

2 Karadeniz Technical University, Trabzon, Turkey

3 Tokyo University of Agriculture and Technology, Tokyo, Japan

References

[1] Deng W, Chen D, Xiong Z, Verlinden P J, Dong J, Ye F, Li H, Zhu H, Zhong M, Yang Y, Chen Y, Feng Z, Altermatt P. 20.8% PERC solar cell on 156 mm × 156 mm P-Type multicrystalline silicon substrate. IEEE Journal of Photovoltaics. 2016;**6**:3–9. DOI: 10.1109/JPHOTOV.2015.2489881

[2] Richards B S. Comparison of TiO_2 and other dielectric coatings for buried-contact solar cells: a review. Progress in Photovoltaics: Research and Applications. 2004;**12:**253–281. DOI: 10.1002/pip.529

[3] Dekkers HF, Beaucarne G, Hiller M, Charifi H, Slaoui A. Molecular hydrogen formation in hydrogenated silicon nitride. Applied Physics Letters AIP. 2006;**89**:211914. DOI: 10.1063/1.2396900

[4] Aberle A, Hezel R. Progress in low-temperature surface passivation of silicon solar cells using remote-plasma silicon nitride. Progress in Photovoltaics. 1997;**5**:29–50. DOI: 10.1002/(SICI)1099-159X199701/02)(5:1<29::AID-PIP149>3.0.CO;2-M

[5] Wan Y, McIntosh KR, Thomson AF. Characterisation and optimisation of PECVD SiNx as an antireflection coating and passivation layer for silicon solar cells. AIP Advances. 2013;**3**:032113. DOI: 10.1063/1.4795108

[6] Brinker CJ, Harrington MS. Sol-gel derived antireflective coatings for silicon. Solar Energy Materials. 1981;**5**:159–172. DOI: 10.1016/0165-1633(81)90027-7

[7] Richards BS. Single-material TiO_2 double-layer antireflection coatings. Solar Energy Materials and Solar Cells. 2003;**79**:369–390. DOI: 10.1016/S0927-0248(02)00473-7

[8] Vitanov P, Loozen X, Harizanova A, Ivanova T, Beaucarne G. A study of sol-gel deposited Al_2O_3 films as passivating coatings for solar cells application. In: Proceedings of the 23rd European Photovoltaic Solar Energy Conference and Exhibition; 1–5 September 2008; Valencia, Spain. pp. 1596–1599. DOI: 10.4229/23rdEUPVSEC2008-2CV.5.5

[9] Liang Z, Chen D, Feng C, Cai J, Shen H. Crystalline silicon surface passivation by the negative charge dielectric film. Physics Procedia. 2011;**18**:51–55. DOI: 10.1016/j.phpro.2011.06.056

[10] Wang MT, Wang TH, Lee JY. Electrical conduction mechanism in high-dielectric-constant ZrO_2 thin films. Microelectronics Reliability. 2005;**45**(5–6):969–972. DOI: 10.1016/j.microrel.2004.11.014

[11] Uzum A, Kuriyama M, Kanda H, Kimura Y, Tanimoto K, Ito S. Non-vacuum processed polymer composite antireflection coating films for silicon solar cells. Energies. 2016;**9**:633–649. DOI: 10.3390/en9080633

[12] Koch W. Properties and uses of ethylcellulose. Industrial and Engineering Chemistry. 1937;**29**(6):687–690. DOI: 10.1021/ie50330a020

[13] Born M, Wolf E. Principle of Optics. 7th ed. Cambridge University Press; Cambridge, UK, 1999. p. 67. ISBN: 0521642221

[14] Kobiyama M. Basic Theory of Thin Film Optics (in Japanese). Optronics Co. Ltd.; 2002. ISBN-10: 4-900-47496-7, ISBN-13: 978-4900474963

[15] Kern W, Puotinen DA. Cleaning solutions based on hydrogen peroxide for use in silicon semiconductor technology. RCA Review. 1970;**31**:187–206.

[16] Reinhardt K, Kern W, editors. Handbook of Silicon Wafer Cleaning Technology. 2nd ed. William Andrew; 2008, Norwich, USA. ISBN: 978-0-8155-1554-8

[17] Uzum A, Kuriyama M, Kanda H, Kimura Y, Tanimoto K, Fukui H, Izumi T, Harada T, Ito S. Sprayed and spin-coated multilayer antireflection coating films for non-vacuum processed crystalline silicon solar cells. International Journal of Photoenergy. 2017;3436271, 5 pages. DOI: 10.1155/2017/3436271

[18] Haque SA, Palomares E, Cho BM, Cho ANM, Hirata N, Klug DR, Durrant JR. Charge separation versus recombination in dye-sensitized nanocrystalline solar cells: The minimization of kinetic redundancy. Journal of the American Chemical Society. 2005;**127**: 3456–3462. DOI: 10.1021/ja0460357

[19] Yu H, Zhang S, Zhao H, Will G, Liu P. An efficient and low-cost TiO_2 compact layer for performance improvement of dye-sensitized solar cells. Electrochimica Acta. 2009;**54**:1319–1324. DOI: 10.1016/j.electacta.2008.09.025

[20] Hocine D, Belkaid MS, Pasquinelli M, Escoubas L, Torchio P, Moreau A. Characterization of TiO_2 antireflection coatings elaborated by APCVD for monocrystalline silicon solar cells. Physics Status Solidi C. 2015;**12**:323–326. DOI: 10.1002/pssc.201400085

[21] Kanda H, Uzum A, Harano N, Yoshinaga S, Ishikawa Y, Uraoka Y, Fukui H, Harada T, Ito S. Al_2O_3/TiO_2 double layer anti-reflection coating film for crystalline silicon solar cells formed by spray pyrolysis. Energy Science and Engineering. 2016;**4**:269–276. DOI: 10.1002/ese3.123

[22] Meiners BM, Holinski S, Schafer P, Hohage S, Borchert D. Investigation of anti-reflection-coating stacks for silicon heterojunction solar cells. In: Proceedings of 29th European PV Solar Energy Conference and Exhibition; 2014. Amsterdam, Netherlands. DOI: 10.4229/EUPVSEC20142014-2AV.3.22

[23] Yu IS, Wang YW, Cheng HE, Yang ZP, Lin CT. Surface passivation and antireflection behavior of ALD on n-type silicon for solar cells. International Journal of Photoenergy. 2013;**431614**:7. DOI: 10.1155/2013/431614

[24] Jhaveri J, Avasthi S, Man G, McClain WE, Nagamatsu K, Kahn A, Schwartz J, Sturm JC. Hole-blocking crystalline-silicon/titanium-oxide heterojunction with very low interface recombination velocity. In: Proceedings of IEEE 39th Photovoltaic Specialists Conference (PVSC); 2013 June; pp. 3292–3296. DOI: 10.1109/PVSC.2013.6745154

[25] Ali K, Khan SA, Jafri MZM. Effect of double layer (SiO_2/TiO_2) anti-reflective coating on silicon solar cells. International Journal of Electrochemical Science. 2014;**9**:7865–7874.

[26] Moradi M, Rajabi Z. Efficiency enhancement of Si solar cells by using nanostructured single and double layer anti-reflective coatings. Journal of Nanostructures. 2013;**3**:365–369. DOI: 10.7508/jns.2013.03.013

[27] Wright DN, Marstein ES, Holt A. Double layer anti-reflective coatings for silicon solar cells. In: Proceedings of the 31st IEEE Photovoltaic Specialists Conference; January 2005; pp. 1237–1240. DOI: 10.1109/PVSC.2005.1488363

[28] Wang WC, Tsai MC, Yang J, Hsu C, Chen J. Efficiency enhancement of nanotextured black silicon solar cells using Al_2O_3/TiO_2 dual-layer passivation stack prepared by atomic layer deposition. ACS Applied Materials & Interfaces. 2015;**7**:10228–10237. DOI: 10.1021/acsami.5b00677

[29] Yang CH, Lien SY, Chu CH, Kung CY, Cheng TF, Chen PT. Effectively improved SiO_2-TiO_2 composite films applied in commercial multicrystalline silicon solar cells. International Journal of Photoenergy. 2013;**823254**:8. DOI: 10.1155/2013/823254

[30] Uzum A, Hamdi A, Nagashima S, Suzuki S, Suzuki H, Yoshiba S, Dhamrin M, Kamisako K, Sato H, Katsuma K, Kato K. Selective emitter formation using single screen-printed phosphorus diffusion process. Solar Energy Materials and Solar Cells. 2013;**109**:288–293. DOI: 10.1016/j.solmat.2012.11.013

[31] Sinton RA, Cuevas A, Stuckings M. Quasi-steady-state photoconductance, a new method for solar cell material and device characterization. In: Proceedings of 25th IEEE Photovoltaic Specialist Conference; Washington DC, USA. 1996. pp. 457–460. DOI: 10.1109/PVSC.1996.564042

[32] Sinton RA, Cuevas A. Contactless determination of current–voltage characteristics and minority-carrier lifetimes in semiconductors from quasi-steady-state photoconductance data. Applied Physics Letters. 1996;**69**:2510–2512. DOI: 10.1063/1.117723

[33] Lossen J, Mittelstadt L, Dauwe S, Lauer K, Beneking C. Making use of silicon wafers with low lifetimes by adequate $POCl_3$ diffusion. In: Proceedings of 20th European Photovoltaic Solar Energy Conference; Barcelona, Spain. 2005. pp. 1411–1414.

[34] Davis Jr, Rohatgi A, Hopkins RH, Blais PD, Rai-Choudhury P, McCormick JR, Mollenkopf HC. Impurities in silicon solar cells. IEEE Transection of Electron Devices. 1980;**27**(4):677–687. DOI: 10.1109/T-ED.1980.19922

[35] Cuevas A, Stocks M, Armand S, Stuckings M, Blakers A, Ferrazza F. High minority carrier lifetimes in phosphorus-gettered multicrystalline silicon. Applied Physics Letters. 1997;**70**(8): 1017–1019. DOI: 10.1063/1.118469

[36] Macdonald D, Cuevas A, Kinomura A, Nakano Y, Geerligs LJ. Transition-metal profiles in a multicrystalline silicon ingot. Journal of Applied Physics. 2005;**97**:033523. DOI: 10.1063/1.1845584

[37] Macdonald D, Cuevas A, Samundsett C, Ferrazza F. Response to phosphorus gettering of different regions of cast multicrystalline silicon ingots. Solid-State Electronics. 1999; **43**(3): 575–581.

[38] Hamdi A, Uzum A, Nagashima S, Suzuki S, Suzuki H, Yoshiba S, Dhamrin M, Kamisako K, Sato H, Katsuma K, Kato K. Phosphorus diffusion impact on carries lifetime of P-type multi- and mono-crystalline silicon wafers using novel screen printed diffusion source. In: Proceedings of 21th Photovoltaic Science and Engineering Conference; December 2011; Fukuoka, Japan. DOI: 10.1016/S0038-1101(98)00283-4

[39] King RR, Sinton RA, Swanson RM. Studies of diffused phosphorus emitters: Saturation current, surface recombination velocity, and quantum efficiency. IEEE Transection of Electron Devices. 1990;**37**(2):365–371. DOI: 10.1109/16.46368

[40] Zhao J, Wang A, Green MA. Emitter design for high-efficiency silicon solar cells. Progress in Photovoltaics: Research and Applications. 1993;**1**(3):193–202. DOI: 10.1002/pip.4670010303

[41] Misiakos K, Lindholm FA. Toward a systematic design theory for silicon solar cells using optimization techniques. Solar Cells. 1986;**17**(1):29–52. DOI: 10.1016/0379-6787(86)90057-8

[42] Haverkamp H, Dastgheib-Shirazi A, Raabe B, Book F, Hahn G. Minimizing the electrical losses on the front side: Development of a selective emitter process from a single diffusion. In: Proceedings of 33th IEEE Photovoltaic Specialists Conference; San Diego, CA, USA; 2008. pp. 430–433. DOI: 10.1109/PVSC.2008.4922443

[43] Meier DL, Schroder DK. Contact resistance: Its measurement and relative importance to power loss in a solar cell. IEEE Transections on Electron Devices. 1984;**31**:647–653. DOI: 10.1109/T-ED.1984.21584

[44] Bähr M, Dauwe S, Mittelstadt L, Schmidt J, Gobsch G. Surface passivation and contact resistance on various emitters of screen-printed crystalline silicon solar cell. In: Proceedings of 19th European Photovoltaic Solar Energy Conference; Paris, France; 2004. pp. 955–958.

[45] Wenham SR, Willison MR, Narayanan S, Green MA. Efficiency improvement in screen-printed polycrystalline silicon solar cells by plasma treatments. In: 18th IEEE Photovoltaic Specialists Conference; Las Vegas, USA; 1985. pp. 1008–1013.

[46] Szlufcik J, Elgamel HE, Ghannam M, Nijs J, Mertens R. Simple integral screenprinting process for selective emitter polycrystalline silicon solar cells. Applied Physics Letters. 1991; **59**(13): 1583–1584. DOI: 10.1063/1.106291

[47] Blendin G, Faber M, Horzel J, Boubekeur H, Metz A. High throughput inline process for deep phosphorus emitters. In: Proceedings of 26th European Photovoltaic Solar Energy Conference; Hamburg, Germany; 2011. pp. 1372–1376.

[48] Hahn G. Status of selective emitter technology. In: Proceedings of 25th European Photovoltaic Solar Energy Conference and Exhibition/5th World Conference on Photovoltaic Energy Conversion; Valencia, Spain; 2010. pp. 1091–1096.

[49] Gauthier M, Grau M, Nichiporuk O, Madon F, Mong-The Yen V, Le Quang N, Zerga A, Slaoui A, Blanc-Pélissier D, Kaminski A, Lemiti M. Industrial approaches of selective emitter on multicrystalline silicon solar cells. In: Proceedings of 24th European Photovoltaic Solar Energy Conference and Exhibition; Hamburg, Germany; 2009. pp. 1875–1878.

[50] Kim IH, Cho KY, Oh DJ, Shim JM, Lee EJ, Lee HW, Choi JY, Kim JS, Shin JE, Lee SH, Lee HS. Exceeding 19% efficient 6 inch selective emitter crystalline silicon solar cell by screen printed metal contacts: transition of heavy & shallow emitter conditions. In: Proceedings of 25th European Photovoltaic Solar Energy Conference and Exhibition/5th World Conference on Photovoltaic Energy Conversion; Valencia, Spain; 2010. pp. 2694–2697.

[51] Koppes M, Stassen AF. Low cost selective emitter for multicrystalline solar cells with 0.4% point efficiency gain. In: Proceedings of 25th European Photovoltaic Solar Energy Conference and Exhibition/5th World Conference on Photovoltaic Energy Conversion; Valencia, Spain; 2010. pp. 1917–1920.

[52] Book F, Braun S, Herguth A, Dastgheib-Shirazi A, Raabe B, Hahn G. The etch-back selective emitter technology and its application to multicrystalline silicon. In: Proceedings of 35th IEEE Photovoltaic Specialists Conference; Honolulu, Hawaii, USA; 2010. pp. 1309–1314.

[53] Low R J, Gupta A, Bateman N, Ramappa D, Sullivan P, Skinner W, Mullin J, Peters S, Weiss-Wallrath H. High efficiency selective emitter enabled through patterned ion implantation. In: Proceedings of 35th IEEE Photovoltaic Specialists Conference; Honolulu, USA; 2010. pp. 1440–1445.

[54] Poplavskyy D, Scardera G, Abbott M, Meisel A, Chen X, Shah S, Tai E, Terry M, Lemmi F. Silicon ink selective emitter process: Optimization of the short wavelength response. In: Proceedings 25th European Photovoltaic Solar Energy Conference and Exhibition/5th World Conference on Photovoltaic Energy Conversion; Valencia, Spain; 2010. pp. 2416–2419.

[55] Röder TC, Eisele SJ, Grabitz P, Wagner C, Kulushich G, Köhler JR, Werner JH. Add-on laser tailored selective emitter solar cells. Progress in Photovoltaics Research and Applications. 2010;**18**:505–510. DOI: 10.1002/pip.1007

[56] Poulain G, Boulord C, Blanc-Pélissier D, Kaminski A, Gauthier M, Semmache B, Pellegrin Y, Lemiti M. Towards a self-aligned process for selective emitters on silicon solar cells. In: Proceedings of 25th European Photovoltaic Solar Energy Conference and Exhibition/5th World Conference on Photovoltaic Energy Conversion; Valencia, Spain; 2010. pp. 2043–2046.

[57] Rudolph D, Peter K, Meijer A, Doll O, Köhler I. Etch back selective emitter process with single $POCl_3$ diffusion. In: Proceedings of 26th European Photovoltaic Solar Energy Conference and Exhibition; Hamburg, Germany; 2011. pp. 1349–1352.

[58] Lee H, Lee EJ, Kim J, Shin J, Kim J, Choi J, Kim I, Shim J, Oh DJ, Cho KY, Kong J, Seo JK, Lee S, Hallam B, Wenham SR, Lee H. Production of 19.2% efficient large area commercial

grade P-type CZ silicon solar cells based on the laser doped selective emitter technology. In: Proceedings of 26th European Photovoltaic Solar Energy Conference and Exhibition; Hamburg, Germany; 2011. pp. 1390–1393.

[59] Lossen J, Jesswein R, Weiß M, Wütherich T, Dupke M, Katkhouda K, Meyer K, Böscke T, Froitzheim A, Eschrich H, Krokoszinski HJ. The DELFIN concept—a screen printed solar cell with >18.5% efficiency. In: Proceedings of 25th European Photovoltaic Solar Energy Conference and Exhibition/5th World Conference on Photovoltaic Energy Conversion; Valencia, Spain; 2010. pp. 2333–2337.

[60] Horzel J, Szlufcik J, Nijs J. High efficiency industrial screen printed selective emitter solar cells. In: Proceedings of 16th European Photovoltaic Solar Energy Conference and Exhibition; Glasgow, UK; 2000. pp. 1112–1115.

[61] Nijs J, Demesmaeker E, Szlufcik J, Poortmans J, Frisson L, De Clercq K, Ghannam M, Mertens R, Van Overstraeten R. Recent improvements in the screen-printing technology and comparison with the buried-contact technology by 2D-simulation. Solar Energy Materials and Solar Cells. 1996;**41/42**:101–117. DOI: 10.1016/0927-0248(95)00136-0

[62] Stem N, Cid M. Physical limitations for homogeneous and highly doped n-type emitter monocrystalline silicon solar cells. Solid-State Electronics. 2004;**48**:197–205. DOI: 10.1016/j.sse.2003.08.005

[63] Blendin G, Faber M, Horzel J, Boubekeur H, Metz A. High throughput inline process for deep phosphorus emitters. In: Proceedings of 26th European Photovoltaic Solar Energy Conference and Exhibition; Hamburg, Germany; 2011. pp. 1372–1376.

IntechOpen